CLM-P732

UKAEA

Preprint

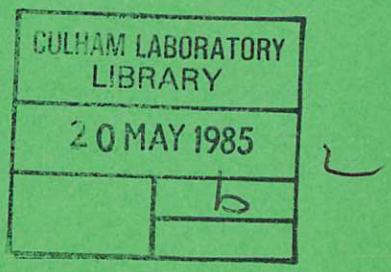

PROBES FOR PLASMA EDGE DIAGNOSTICS IN MAGNETIC CONFINEMENT FUSION DEVICES

D. M. MANOS
G. M. McCRACKEN

CULHAM LABORATORY
Abingdon Oxfordshire

1985

CLM-P 732

PROBES FOR PLASMA EDGE DIAGNOSTICS IN MAGNETIC CONFINEMENT FUSION DEVICES

D. M. Manos* and G. M. McCracken

Culham Laboratory, Abingdon, Oxon, OX14 3DB, U.K.
(UKAEA/Euratom Fusion Association)

ABSTRACT

Probes are becoming widely used in fusion devices to measure edge plasma parameters. Both electrical probes and surface collector probes can provide useful data and the two techniques are largely complementary. Energy analysers are included among the electrical probes and long term probes placed on the walls for extended periods are included in the surface probes. Methods of measuring erosion and redeposition are also outlined. Some of the problems inherent in probes such as disturbance of the plasma and practical problems of construction are discussed.

* Plasma Physics Laboratory, Princeton University, Princeton, New Jersey 08544, U.S.A.

To be published in Proceedings of NATO Advanced Study Institute on Plasma Surface Interactions held at Val Morin P.Q., Canada, August 1984. (Editors R. Behrisch and D. Post.)

PROBES FOR PLASMA EDGE DIAGNOSTICS IN MAGNETIC CONFINEMENT FUSION DEVICES

D.M. Manos and G.M. McCracken

Contents

1. INTRODUCTION

The use of solid probes to measure plasma parameters has a history going back at least to Langmuir[1]. Their use in tokamaks however has been limited until relatively recently, partly because of the difficulty involved in their proper deployment, and partly due to uncertainty in the interpretation of probe data. There is no doubt that probes affect the plasma and the plasma flux affects the probes. Each of these complex interactions has to be understood if a reliable interpretation of what is happening at the boundary is to be obtained. The presence of surfaces in the plasma boundary as limiters, walls or as divertor neutralizer plates is inevitable. One can make probes large so that they simulate such components or one can make probes small so that they cause the least disturbance possible to the plasma. In either case modelling

is necessary in order to interpret the results in terms of the plasma surface interaction.

Probes can be broadly divided into two categories, electrical probes (e.g. Langmuir probe) and surface collector probes. A list of some examples of the two types of probes and the parameters they may potentially measure is given in Table 1. We define electrical probes to include any probe which uses an electrical measurement technique, so the term encompasses gridded energy analysers, ExB probes, heat flux probes, etc. They can, in principle, measure the saturation ion flux, the power deposited, electron and ion temperatures and hence can be used to evaluate the plasma density. At present no electrical probe has been developed which can measure impurities directly, although mass spectrometer techniques are possible. Collector probes, on the other hand are able to detect impurities directly. They rely on exposing a clean, well-characterized surface to the plasma for a known length of time and then removing the sample for analysis using one or more of the wide range of the surface analytical techniques. From the collected number of a given species of atom and the exposure time, the average incident flux can be obtained. The technique is also of value in distinguishing between different hydrogen isotopes. In this case it has been shown that the energy of the ions at the surface can be inferred by measuring the depth distribution of the implanted species. This approach also has considerable potential for determining both the flux and energy distribution of escaping α particles in DT burning plasmas. In order to fully interpret measurements with surface probes it is necessary to have independent measurements of the edge plasma parameters as well. So in most respects the two techniques, electrical measurement and surface analyses, should be looked on as complementary rather than as alternative methods of measuring plasma edge properties.

2. EFFECT OF THE PLASMA ON THE PROBES

One of the first considerations is the type of plasma which may be safely accessed by the probe. It is clearly necessary to avoid excessive heat loads on the surface of a collector in order to avoid evaporation of the collected species or diffusion of it into the bulk of the material. This requirement is most severe when attempting to determine the incident hydrogen flux and energy in collector probes, since the trapped hydrogen can be thermally released. The tolerable heat load on an electrical probe will be higher than for a collector probe, as it is normally only necessary to prevent evaporation or thermionic emission from occurring. The temperature rise of a surface is determined mainly by heat conduction into the bulk since radiation is often negligible for the conditions of interest. The temperature rise can be calculated by solution of the heat conduction equation. The solution for the

Table 1. Type of Probes and Parameters Measured

Electrical Probes	Parameter	Surface Collector Probes	Parameter
Langmuir Probes		Surface analysis	
single	n_e T_e V_f	Impurity mass and flux	Γ_I
double	n_e T_e	Plasma flux and energy	$\Gamma_H, \Gamma_D, \Gamma_T, T_i$
triple	n_e T_e V_f		
Larmor radius probes	T_i	Thermal desorption probe	$\Gamma_H, \Gamma_D, \Gamma_T, T_i$
Energy analysers		Alpha particle flux	Γ_α,
Gridded	$N_e(E)$		
	$N_i(E)$	Metal surface collectors	$N_\alpha(E)$
ExB	$N_i(E)$		
		Erosion	
In situ mass spectrometers		Thin film or implant marker	
Impurity flux	Γ_I	Thin film activation	
Hydrogen flux	$\Gamma_H, \Gamma_D, \Gamma_T$	Weight loss Collectors	
Heat flux probe		Macroscopic measurement	
Power	P_D		
Partial pressure probes	$\Gamma_H, \Gamma_D, \Gamma_T$		
Carbon resistance probe	Γ_H, T_i		

n_e	electron density
V_f	floating potential
T_e, T_i	electron and ion temperature
P_D	deposited power
$N_e(E)$, $N_i(E)$	electron and ion energy distributions
Γ_I, Γ_H, Γ_α	flux of impurities, hydrogen, α particles.

surface of a semi-infinite solid at a time t after the start of a constant power flux P is[2]

$$\Delta T = 2P\sqrt{t/(\pi KC\rho)} \qquad (1)$$

where K is the thermal conductivity, C the specific heat and ρ the density of the solid. The condition that a solid has a thickness, d, large enough to behave like a semi-infinite solid is

$$t < \frac{d^2 \rho C}{4K}. \qquad (2)$$

(The parameter $D = K/\rho C$ is known as the thermal diffusivity and, for heat diffusion, is the direct analog of the diffusion coefficient in kinetic theory). Materials with good thermal constants are C, Cu, Mo, W. Values of the thermal constants are shown in Table 2. It is seen that carbon, molybdenum and tungsten are comparable. A heat flux of < 500 watts cm^{-2} for 1 sec is tolerable if a surface temperature rise of 300°C is not to be exceeded. As discussed later in sections 4.2 and 4.3, other criteria favour carbon as a collector surface. It is seen that pyrolytic carbon has good thermal properties in the direction parallel to the basal plane, although it is very anisotropic. Its thermal conductivity is particularly good at low temperature and it is therefore ideal for collector probes where it is desirable to keep the surface as cool as possible cf. chapter by Smith and Whitely. Copper is an undesirable material close to the plasma because of its high sputter yield and relatively high atomic number.

Table 2. Tolerable Heat Fluxes for Probes

Material	$\sqrt{\pi KC\rho}$ at 300 -1000K	D $cm^2 s^{-1}$ at 300 -1000K	ΔT_1* K	Tolerable Heat Flux for 1 sec: kW cm^{-2} for ΔT_1	kW cm^{-2} ΔT=300K	Heat capacity for 1mm J cm^{-2}
W	3.3	0.72	2400	4.0	0.5	700
Mo	3.3	0.56	1800	3.0	0.5	560
C(ATJ)	2.9	1.1	1730	2.7	0.43	740
C(Pyrolytic)∥	10.4	12.3	1730	9.7	1.5	740
C(Pyrolytic)⊥	0.7	0.059	1730	0.65	0.1	740
SS	1.0	0.043	1000	0.5	0.15	430

* Temperature rise to that temperature at which the vapour pressure is 10^{-6} torr.

For reactor relevant plasmas the pulse length will be much in excess of 1 sec and therefore it is clear that if the critical temperature is not to be exceeded only much lower power levels can be tolerated. There are two approaches to this problem. One is to design a collector which is actively cooled. It can be shown[3] that active cooling, rather than inertial cooling, is appropriate for pulse lengths $\gtrsim$ 10 sec. Clearly if limiters are going to withstand heat loads in reactors then collectors can also be made to do so. However, active cooling of probes will cause significant technical problems. The other approach is to use moving collectors for short times. Either the collector surface can be exposed for a short time and then withdrawn from the plasma or else used as a time-resolved collector rotating behind an aperture. In either case exposure times of 0.1 sec can be easily obtained, increasing the tolerable heat flux by a factor of 3.

We must now consider the plasma conditions accessible to such collectors. The heat flux to a surface is discussed in detail in section 3. It depends strongly on the potential of the surface with respect to the plasma, and is nearly a minimum for the floating potential. The incident power flux P is given in this case by

$$P = \delta \, I_s^+ \, kT_e . \qquad (3)$$

where δ is the sheath energy transmission factor, I_s is the ion saturation current given by $I_s \sim 0.5 \, n_e C_s A$, n_e is the plasma density, A is the probe area and C_s is the ion sound speed given by

$$C_s = \sqrt{k \, (T_e + T_i)/m_i} \qquad (4)$$

and T_i and T_e are the ion and electron temperatures respectively. The sheath transmission factor is a complex function which depends on the ratio of T_i/T_e, on secondary electron emission coefficients γ, and on the probe potential with respect to the plasma. For a floating probe, with $T_i/T_e = 1$, and $\gamma = 0.6$, δ is typically ~ 8 for hydrogen. This is made up of 2 kTe each from ions and electrons, $\sim 3 \, kT_e$ due to the sheath potential and ~ 0.5 kTe from the presheath. This subject is discussed in more detail elsewhere (see chapters by Stangeby and Chodura). From (3) using the values for I_s and C_s we obtain

$$P = 1.1 \, \delta \, n_e \, T_e^{3/2} \, (1 + T_i/T_e)^{1/2} \text{ watts cm}^{-2} \qquad (5)$$

for n_e in units of 10^{13} cm^{-3} and T_e and T_i in eV. Normally we have a limitation on the maximum power P_c a material may intercept for a given length of exposure time, e.g. as in Table 2. We thus can rewrite (5) in the form

$$n_c < P_c (1.1 \, \delta \, T_e^{3/2} \, (1 + T_i/T_e)^{1/2})^{-1} . \qquad (6)$$

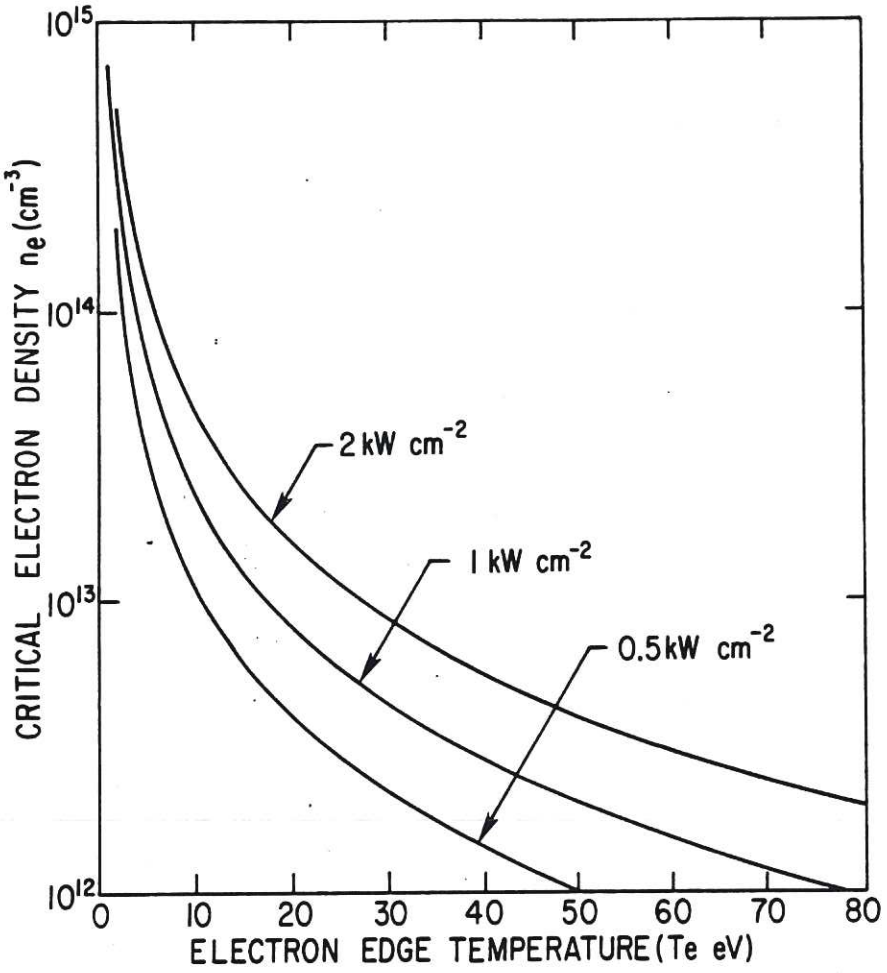

Fig. 1 Maximum plasma density for probe operation as a function of plasma temperature for power fluxes of 0.5, 1.0 or 2.0 kW cm^{-2} ($T_e = T_i$ is assumed).

We can then calculate the critical density n_c which should not be exceeded for a given value of T_e. Results are shown in Fig. 1. As the edge temperature increases the tolerable density decreases. Fortunately in practice as the edge density rises the temperature tends to drop thus allowing a reasonably wide range of plasmas to be investigated. A further factor that has to be taken into account is that at low incident ion energies there is a significant fraction of the ion energy backscattered rather than deposited in the solid, see Behrisch (these proceedings). This reduces the heating of the solid. In the case of tungsten at low ion energies the effect can reduce the deposited heat flux by 50%, but in low Z materials such as carbon the correction is much

smaller. This effect has to be taken into account when comparing measured heat flux with plasma parameters.

3. ELECTRICAL PROBES

3.1 Single Langmuir Probe

A Langmuir probe is a conductor immersed in a plasma which may be biased relative to a second conductor (counter electrode, wall, limiter, etc.) in contact with the plasma. The theory of the development of the sheath and presheath is developed fully by Stangeby and Chodura (these proceedings). We recall a few essential results in this section. The theory of probes in general is discussed in a number of standard texts[4,5,6].

In the simple theory of a Langmuir sheath the high velocity of electrons compared to ions causes an electrically isolated surface to charge negatively with respect to the plasma. The sheath potential V_f is set up when the probe is floating, that is, when it may draw no net current, forcing the electron and ion fluxes to the surface to be equal. For $T_i = 0$ this result can be written as

$$V_f = \frac{kT_e}{2e} \ln \left(\frac{m_i}{2\pi m_e}\right), \qquad (7)$$

where e and m_e are the electron charge and mass and m_i is the positive ion mass. For a hydrogen plasma $V_f \sim 3k\ T_e/e$. The presence of a sheath acts as a thermal barrier by reducing the electron conduction and hence the heat flow, by as much as a factor of 10. It also accelerates the ions into the wall with energies exceeding their thermal energy. In the case of multiply charged ions this can result in a considerable increase in the sputtering rate. As T_e increases the ions and electrons arriving at the surface can produce secondary electrons which will tend to reduce the potential. A model taking into account secondary electron emission but with $T_i = 0$ has been discussed by Hobbs and Wesson[7]. A fuller treatment of the problem has been discussed by Harbour and Harrison[8].

Where the singly charged ions have a finite temperature it is still possible to get a simple form for the sheath potential if it is assumed that the electron energy distribution remains Maxwellian[9]. The electron and ion current densities to the surface are given by

$$j^- = \frac{1}{4} n_e c_e e(1 - \gamma_e) \exp\left(-\frac{eV}{kT_e}\right) \qquad (8)$$

$$j^+ = n_e c_s e$$

where

γ_e = secondary electron emission coefficient

$c_e = (8\ kT_e/\pi\ m_e)^{1/2}$

$c_s = (k\ (T_e + T_i)/m_i))^{1/2}$

V = potential between the plasma and the surface,

and n_e is the density of the electrons (or ions) at the sheath boundary. It can be shown that n_e at the boundary is approximately equal to 1/2 of its value in the unperturbed plasma at a large distance (say 100 debye lengths) from the probe surface.

At the floating potential the electron and ion currents must be equal and we thus obtain

$$1/4\ n_e c_e e\ (1 - \gamma_e) \exp\left(\frac{-eV_f}{kT_e}\right) = n_e c_s e$$

or

$$V_f = -\frac{kT_e}{2e}\ \ln\left[\frac{2\pi m_e}{m_i}\ (1 + T_i/T_e)/(1 - \gamma_e)^2\right] \qquad (9)$$

where we have only included the electron impact secondary electron emission coefficient. The complete calculation has been made by Harbour taking into account the correct electron energy distribution[10]. However, the calculation is much more complex and the result obtained in the simplified treatment is very similar.

Up to now we have been considering the floating potential of a passive surface. We must remember that the plasma is normally electrically connected to earth via the limiter (or wall). It will therefore float at some potential with respect to this surface. This potential cannot be precisely defined because the limiter potential is an average of a complicated spatial variation of sheath potential since it is exposed to the profile variation of n_e and T_e. We also note that the floating potential of an object in a strong magnetic field depends upon its size (see Stangeby these proceedings). This results from the fact that electrons and ions have greatly different gyroradii. The different gyro radii affect the ratio of parallel and perpendicular mobility of the species and also change the apparent probe collection area for ions and electrons. So although a floating probe will take a value for its potential which is mainly determined by its local T_e, it will not in general be the same as the limiter potential. It is frequently found that in scrape-off plasmas the floating potential of probes relative to the limiter is less than 10 volts[11].

A probe in the plasma may have potential applied, say with respect to the limiter. It can therefore be driven up or down with respect to the plasma potential from its floating potential. When driven sufficiently negative it will repel all electrons and the current density arriving will just be the ion saturation current density

$$j_{sat} = n_e e\, c_s. \qquad (10)$$

The general expression for the net current density to the probe $j = j^+ + j^-$, hence

$$j = j^+ + j^- = n_e e\, C_s - 1/4\, n_e e\, C_e\, (1 - \gamma_e)\, \exp\left(\frac{-eV}{kT}\right), \qquad (11)$$

where V is the difference between the potential of the plasma and the probe. In Fig. 2, we show a representative single Langmuir probe characteristic. The zones of behaviour may be described heuristically as follows:

Region C: $V \ll 0$:

In this region all of the electrons are repelled and all of the ions are collected. The ions are accelerated in the presheath by the applied voltage and the sheath thickness itself is affected slightly by the applied voltage. Thus there is only a weak dependence on voltage and the formula for "ion saturation" applies.

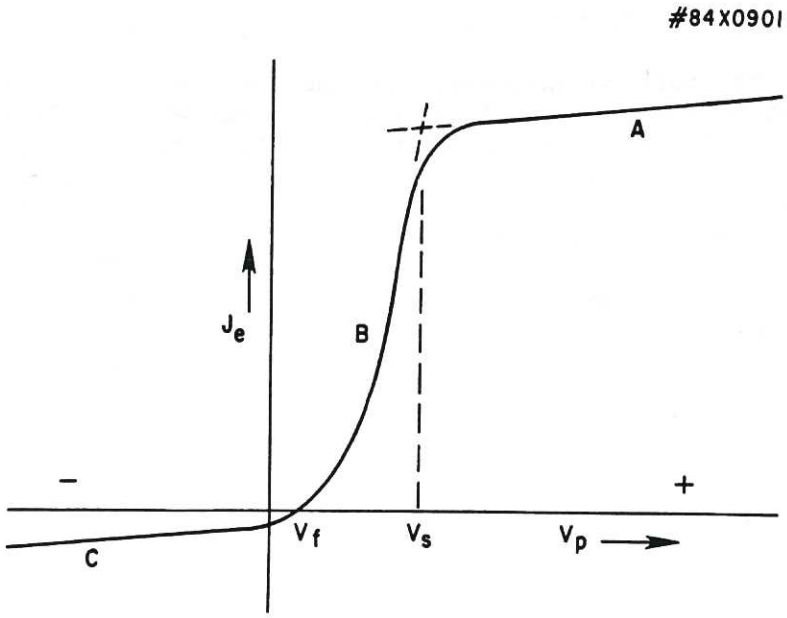

Fig. 2 Schematic of Langmuir probe characteristic illustrating the floating potential V_f, space potential V_s.

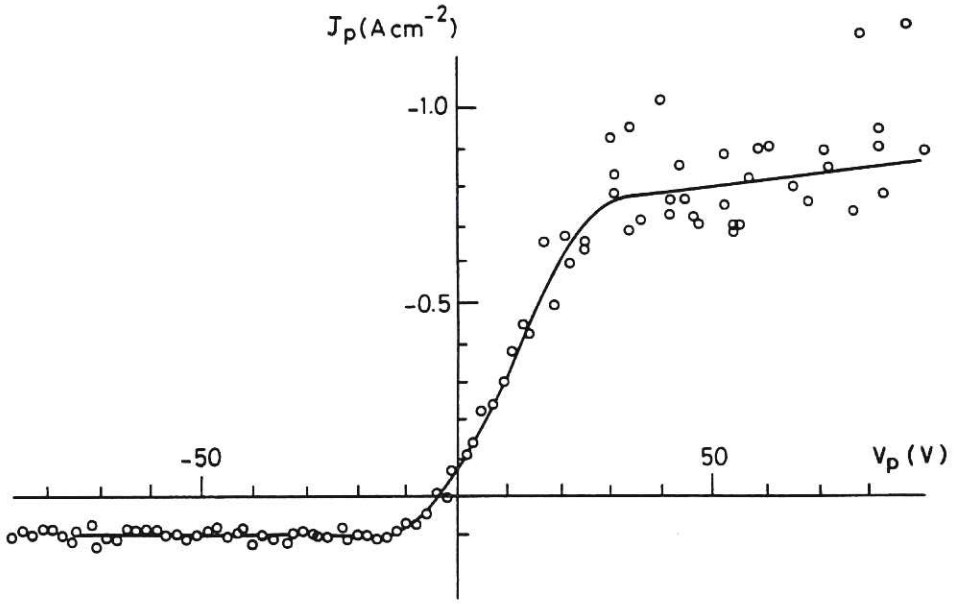

Fig. 3 Langmuir probe characteristic taken in the DITE tokamak with plasma current = 120 kA, toroidal field = 2T and the probe 35 mm behind the limiter.

Region B: $V_f \sim V < V_s$:

As the voltage increases some of the electron distribution is admitted to the probe. The floating potential, V_f, is then achieved and the net current is zero. As V continues to rise an exponential increase in the electron current is observed, as governed by the second term of Eq. (11). It is from this zone that T_e may be computed from the slope of $\ell n(j-j_{sat})$ vs V.

V_s: As V rises further the probe reaches the potential of the plasma, also called the "space potential" and designated V_s, the exponential term vanishes and the entire random electron current is admitted.

Region A: $V > V_s$:

Above V_s one again sees only a slow dependence of current density on applied voltage as the presheath attraction slowly reaches further into the bulk plasma. This is the "electron saturation" regime. In a strong magnetic field the electron saturation current can be significantly reduced compared to the zero field case. This is due to depletion of electrons in the flux tube connected to the probe and the low cross field diffusion

rate of electrons. It is discussed in more detail in section 5.1 and by Stangeby and Chodura (these proceedings).

An experimental Langmuir probe characteristic taken on a tokamak with the torus as the reference potential is shown in fig. 3. It is seen that the ion saturation current is very flat to at least - 100 volts. The floating potential is negative with respect to the torus. The noise in the electron saturation current is due to fluctuations; this is typical of behaviour in tokamak boundaries as is the rather low ratio of electron to ion saturation current. It should be noted that a probe can only be driven to electron saturation when it is some distance outside the limiter radius otherwise the current drawn and the power deposited will be excessive.

Langmuir probes have now been used in large numbers of tokamaks[12-18] and increasing use is being made of large arrays of 50 or 60 probes to investigate poloidal variations of plasma edge characteristics[19,20].

3.2 Double Langmuir Probe

There are times when a single probe may be difficult to use. For example, there may be no well-defined counter-electrode (ground) plane as in the case of an electrodeless rf induced plasma in a dielectric container. There may be prohibitively large fluctuations in V_s induced by waves or turbulence in the plasma. These lead to noise in the current which result in large uncertainties in T_e. There are also cases where the plasma is dilute or otherwise easily perturbed and drawing large electron saturation currents is undesirable. In these instances one may employ a double Langmuir probe[21,22] as shown schematically in Fig. 4a.

The double probe uses a small counter electrode as the reference for the return current and the entire system floats at a potential dictated by V_s and T_e. This is shown schematically in Fig. 4b for the case of $V_1 - V_2 > 0$.

The current voltage characteristic equation may be developed by treating each electrode as a single probe, adding the con straint that the system floats, i.e.,

$$j_1 + j_2 = 0 \qquad (12)$$

and

$$V_2 = V_1 - V \qquad (13)$$

Thus one arrives at the expression relating the applied

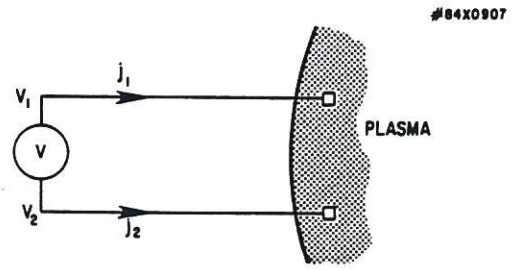

Fig. 4a Schematic of Langmuir double probe.

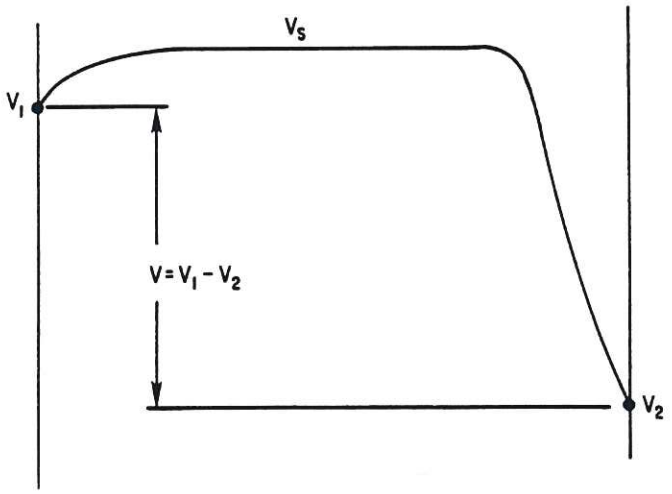

Fig. 4b Potential diagram for the above probe when $V_1 >> V_2$.

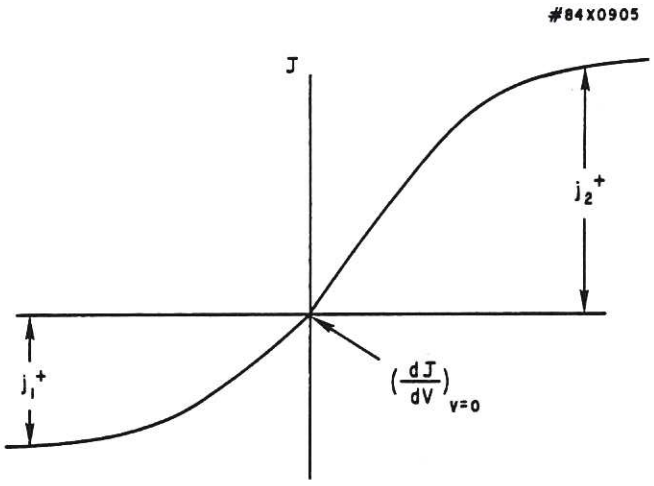

Fig. 4c Representative double probe characteristic.

potential, V, and the actual electrode potential V_1:

$$\exp\ (eV_1/kT_e) = \frac{2\exp\ (eV_f/kT_e)}{1 + \exp\ (-eV/kT_e)} \cdot \qquad (14)$$

This may be substituted into the expression for the current on electrode 1 and electrode 2 to develop the general characteristic:

$$\frac{J + j_1^+}{j_2^+ - J} = \frac{A_1}{A_2} \exp\ (eV/kT_e) \qquad (15)$$

where J is the current in the external circuit, (j_1 or $-j_2$). j_1^+ j_2^+ are the ion saturation currents for electrodes 1 and 2 respectively, i.e., the current observed when $V_1 \ll V_2$ and vice versa.

and A_1 and A_2 are the collection areas of electrode 1 and 2 respectively.

A representative double probe characteristic is shown in Fig. 4c. Differentiating (15) we find

$$\left[\frac{dI}{dV}\right]_{V=0} = \frac{e\ (j_1^+)(j_2^+)}{kT_e\ (j_1^+ + j_2^+)} \cdot \qquad (16)$$

We note that in the commonly employed special case of $A_1 = A_2$ (therefore $j_1^+ = j_2^+$) the characteristic may be written

$$j_1 = j_+ \tanh\ \left(\frac{eV}{2kT_e}\right) \qquad (17)$$

and differentiating yields

$$\frac{kT_e}{e} = \frac{j_+}{2(dJ/dV)_{V=0}} \cdot \qquad (18)$$

T_e is extracted quite easily from the slope of J vs V at V = 0. As for the single probe, n_e is derived from the ion saturation value, the calculated T_e, and the assumed, or independently measured, T_i.

The principal disadvantage of the double probe is that because both electrodes are floating it only samples the tail of the electron energy distribution. For equal area electrodes it samples ~ 14% of the distribution, thus if the distribution is non-Maxwellian erroneous temperatures can be derived. For an asymmetric probe a larger fraction of the distribution is sampled, depending on the ratio of the areas and the ratio of the ion to

electron saturation current. Asymmetric double probes have been used routinely on DITE[23]. A further drawback of the double probe is that the floating potential is not measured. However this is easily overcome by using the triple probe.

3.3 Triple Probe

A further modification of Langmuir probes involves adding a third electrode in close proximity to a double probe. This electrode is used to independently measure the floating potential and the entire configuration is called a triple probe[24,25]. Taking the double probe analysis above, we have the result of equation (14)

$$\exp\,(eV_1/kT_e) = \frac{2\,\exp\,(eV_f/kT_e)}{[1 + \exp\,(-\,eV/kT_e)]}\,, \qquad (19)$$

where $V = V_1 - V_2$. Suppose we set the applied potential so that $V \gg kT_e$ then from above we obtain

$$\frac{eV_1}{kT_e} = \frac{eV_f}{kT_e} + \ell n2 \qquad (20)$$

or

$$\frac{kT_e}{e} = \frac{1}{\ell n2}\,(V_1 - V_f). \qquad (21)$$

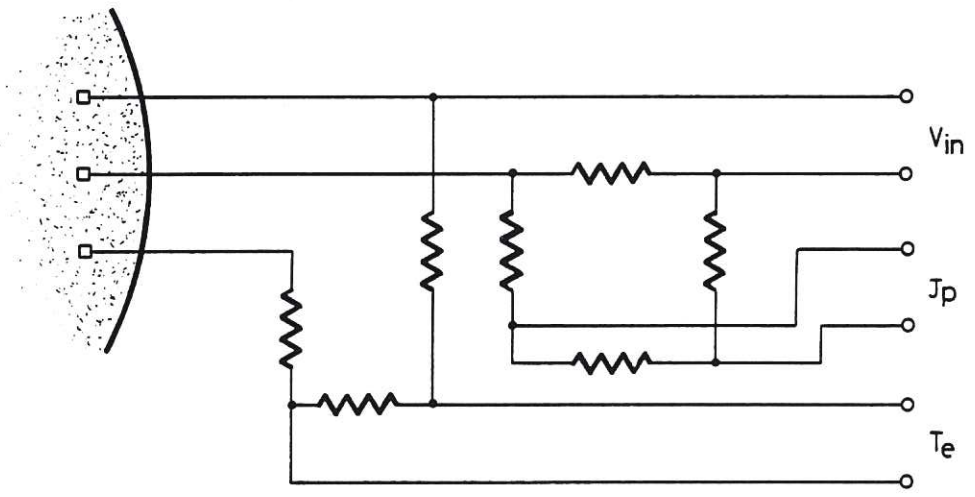

Fig. 5 A simple circuit for measuring the ion probe current and the electron temperature using a combination of a double probe and floating probe[26].

A measurement of the voltage between the positive double probe electrode and the floating electrode yields T_e directly. This can be done by means of a simple electrical circuit[26] as shown in fig. 5. Fig. 6 shows a comparison of T_e derived from the triple probe analysis to that derived from double probe analysis on PDX. The agreement is quite good. A detailed comparison of double and triple probes in magnetic fields has been given by Budny and Manos[16].

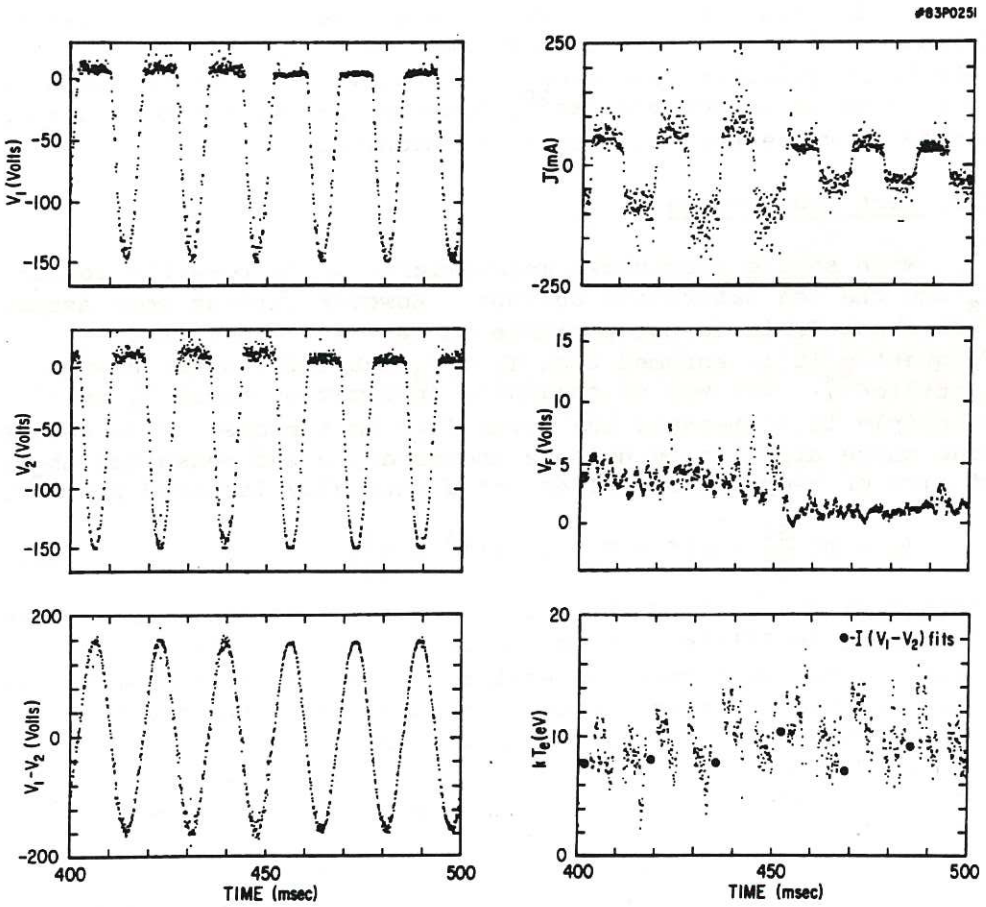

Fig. 6 A comparison of double and triple probe behaviour. The applied voltage (lower left) is measured relatively to the vacuum vessel wall and resolved into two components V_1, V_2. The electron current j, (upper right) and independently measured floating potential on the third wire (middle right) are also shown. At lower right is shown the directly read T_e from the triple probe superimposed on T_e (0) calculated from the double probe characteristics.

3.4 Other Langmuir-like Probes

Another variant on the Langmuir probe is the electron emitting probe[27]. By operating the probe at an elevated temperature, it will emit electrons whenever the probe potential equals or exceeds the plasma potential. The plasma potential can be derived by comparing the current-voltage characteristics of the probe when hot and cold. However operating at positive potential results in high heat flux. Such probes are inherently physically delicate and until recently have been generally of use only in relatively quiescent low density plasmas. They can be constructed to survive in denser plasmas[28], however, and with modifications may be of value even in long pulse machines.

3.5 Heat Flux Probes

With simple electrical measurements it is possible to obtain T_e and the ion saturation current. However without some assumption about T_i it is not possible to derive the density. Frequently it is assumed that $T_i = T_e$ but this is not always justified[29]. One way of obtaining information about T_i in principle is to measure the power (P_D) to a probe. This can be done quite directly by using a thermocouple and measuring the rate of rise of temperature (dT/dt) of a thermally isolated probe[30].

$$P_D = mC \frac{dT}{dt} + \alpha(T - T_B) + \varepsilon\sigma(T^4 - T_B^4) \qquad (22)$$

where m is the mass, C the specific heat, α is the thermal conduction drain coefficient, ε the emissivity, σ the Stefan-Boltzman constant, T_B the vessel temperature and T the probe temperature. α can be obtained from the cooling curve after the discharge. For short pulses heat loss by conduction and radiation can often be neglected. By using a material with high thermal conductivity such as tungsten or molybdenum it is quite straightforward to obtain thermal time constants of ~ 1-10 ms. Electrical noise due to inductive effects can be largely eliminated by careful twisting of leads. However noise from the plasma can be a problem, sometimes requiring integration times of > 100 ms to average out the noise.

A heat flux probe is shown in Fig. 7a. Fig. 7b indicates the maximum operating boundary in the power vs time plane for particular choices of thermocouple types.

The power P_I arriving at a probe at floating potential is given for singly charged ions by

$$P_I = I_s kT_e \left\{2(T_i/T_e) + 2(1 - \gamma_e)^{-1} + eV_f/kT_e\right\} \qquad (23)$$

where we have neglected the ion neutralization energy.

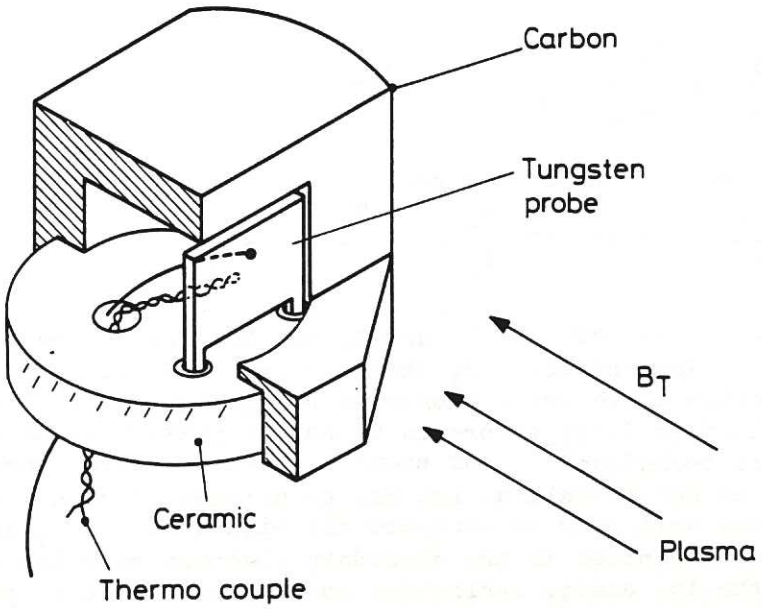

Fig. 7a The combined heat flux probe and single Langmuir probe construction.

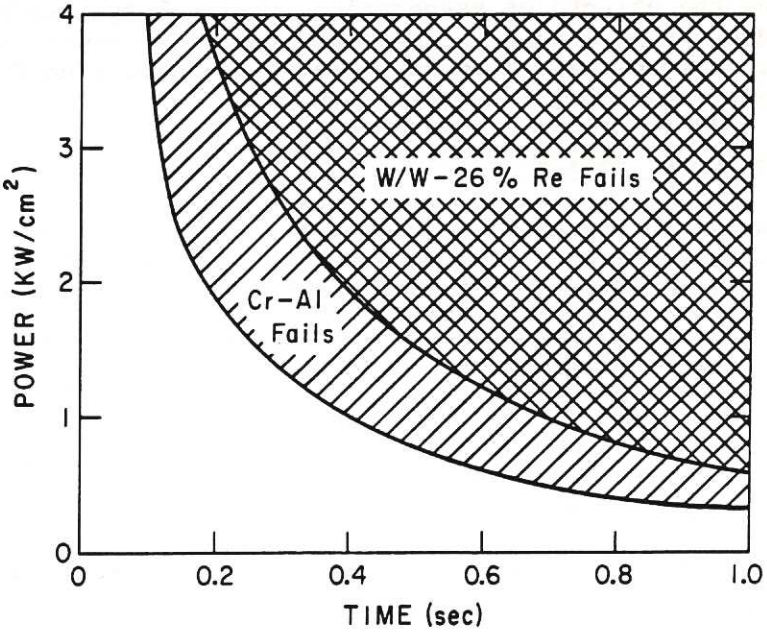

Fig. 7b Calculated operating boundary for a 1 mm thick Ta collector plate. In the unshaded region the probe operates normally. In the single shaded region a chromel alumel thermocouple will melt. In the doubly shaded region a W/W-26% R_e thermocouple calibration fails but the device is not destroyed.

Hence

$$\frac{T_i}{T_e} = \frac{eP_I}{2kT_e I_s} - \frac{eV_f}{2kT_e} - \frac{1}{1 - \gamma_e} \qquad (24)$$

We also have from Eq. (9) that

$$\frac{eV_f}{kT_e} = - 1/2 \ln \left[2\pi \left(\frac{m_e}{m_i}\right)\left(1 + \frac{T_i}{T_e}\right) (1 - \gamma_e)^{-2}\right]. \qquad (25)$$

From Eqs. (24) and (25) T_i and V_f can be obtained by successive approximation and hence T_i obtained independently of T_e. However in practice there are a number of uncertainties in this derivation which lead to large errors in T_i and at present it is not a very reliable technique[17]. For example if the electron energy distribution is not Maxwellian but has an unexpected high energy component this will give an unexpectedly high value to P_I and hence to T_i. Uncertainties in the secondary electron emission coefficient or in the ion energy reflection coefficient can also produce substantial errors in the calculated value of T_i. Thus the use of the measured power to the probe to calculate T_i must be used with caution. The technique however, is useful for measuring surface temperature since this parameter is inherently of interest for estimating the effects of evaporation, chemical sputtering, thermal desorption, etc. The measured deposited power is also a useful cross check on the power incident as calculated from independently measured plasma parameters.

3.6 Mach Number Measurements

From a simple analysis of the scrape off layer radially outside the limiter it is easy to show that there will be a stagnation point between the limiters and that the ions will acquire a net drift velocity as they come near to the limiter, (see Stangeby, these proceedings). There will thus be a difference between the flux arriving at a probe placed a distance from the stagnation point, depending on whether it is facing upstream or downstream. The Mach number (M) of the plasma is defined as the ratio of the drift velocity to the sound speed c_s. Under simple conditions the Mach number will increase from zero at the stagnation point to 1 at the sheath edge (according to the Bohm criterion). Taking the fluid model for $M < 1$ we get a simple form for the ratio of the flux in the upstream to downstream direction[31]

$$\frac{\Gamma_u}{\Gamma_d} = \frac{2 - M}{2 + M}$$

e.g. for $M = - 0.5$ $\Gamma_u/\Gamma_d = 5/3$

Thus by measuring R the Mach number can be deduced. This technique has been used by Harbour and Proudfoot[32] using 2 double probes facing both directions simultaneously. Significant asymmetries were observed which were interpreted as being due to this flow and Mach numbers deduced. There are however a number of difficulties with this interpretation. Kinetic and fluid models give significantly different results so that the Mach number deduced is model dependent. Both models give unrealistic behaviour for $M > 1$ so that it is only possible to deduce that flow is supersonic - not what the actual Mach number is. Finally processes other than flow to the limiter can cause plasma drift e.g. plasma rotation due to ion beams or rf heating. Thus at present this technique has to be treated with considerable caution.

3.7 Partial Pressure Probes

A completely different approach to measuring ion flux is shown in fig. 8. An aperture defines the incident flux which enters a small chamber and thermalizes by collisions with the internal surfaces. The partial pressure rise in the chamber is proportional to the incident flux. Although it is not strictly speaking an electrical probe it is a direct reading device and so is included in this section. If we consider the probe to be floating and the chamber to be unpumped except for the aperture then

$$\Delta P = \frac{\Gamma_s}{C} = \frac{\Gamma_{s\sqrt{M/2}}}{440} \text{ torr}$$

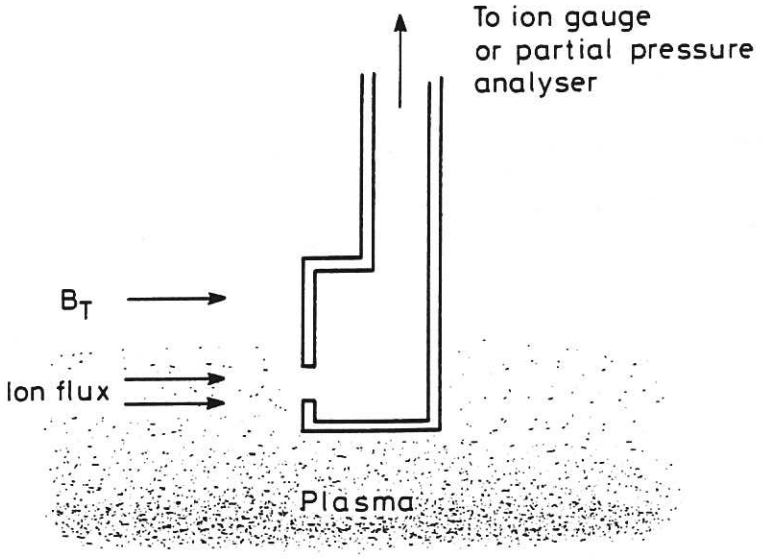

Fig. 8 Schematic of a pressure probe for measuring ion flux.

where Γ_s is the ion saturation current in amps cm^{-2}, M is the molecular weight of the incident ion, and we have assumed that the aperture is thin and its conductance C is proportional to its area. Thus a large pressure rise is predicted even for currents at the mA cm^{-2} level. The pressure rise could be enhanced by reducing the conductance using a thick aperture or decreased by adding additional pumping. It is clearly possible to measure this pressure rise using a partial pressure analyser and so to distinguish between hydrogen isotopes and possibly other gaseous species. The technique has been applied to ASDEX[33]. The practical difficulties include getting a partial pressure analyzer sufficiently close to the machine, to reduce the time constant of the vacuum system to make real time measurements during a discharge and at the same time to shield the instrument from electrical and magnetic interference. Another problem is the interpretation of the pressure rise as there is the possibility of either trapping and loss of the incident species or desorption of other gas at the internal surfaces of the chamber. The problems are similar to those in measuring ion beam trapping mass spectrometrically[34]. Conditioning the surface by heating and using repeated discharges until reproducible conditions are obtained can enable a measure of the incident ion flux to be obtained. A further difficulty is that the conductance of the hole for the thermalized species may be reduced by the flux of energetic particles entering the chamber, so-called "plasma plugging". This process is expected to be highly non-linear with little effect at low density and a strong effect at high density. The situation is similar to that for pumped limiters. In pumped limiter experiments on ISX good agreement was obtained between the ion saturation current and the pressure rise[35] with Γ_s in the range 1 to 2 amps cm^{-2}.

3.8 Complications in the Use of Probes

There are numerous complications that arise in the use of probes to diagnose fusion plasmas. An obvious source of trouble is the difficulty involved in the experimental design, construction, and deployment of probes. We defer this topic to the end of this chapter.

Probes are intrinsically perturbing to the distributions they attempt to measure. Probes collect particles in a certain portion of phase space and reflect others, thereby modifying distributions. As discussed by Stangeby[36] the existence of a sheath implies a modification of the plasma density and electric field at its boundary. The electric field in turn seriously modifies the ion distribution at the probe location. Simple estimates of the degree to which a probe intrinsically perturbs the plasma are possible[37]. If the probe collector dimensions, d, become comparable to the collisional mean free path λ_{mfp}, i.e. $d/\lambda_{mfp} \sim 1$, the probe

will seriously distort the distribution function of the collected species. If the net probe current drawn is comparable to the volume plasma source rate, the probe is more seriously perturbing. This latter condition rarely applies to modern fusion devices, nevertheless large probes may still seriously affect the density of a strongly magnetized plasma over long parallel distances (see Section 5.1 of this chapter). Stangeby has given an analysis of the various distortions which may occur for large probes[38]. Fortunately it is possible to correct scrapeoff lengths of n_e, T_e, and power extracted from measurements of radial variations rather easily. The analysis also indicates that when a probe is operated in front of a limiter or "back stop", interpretation of the data is facilitated.

As probes are deployed in hotter, denser regions of the plasma, the plasma-surface interactions discussed earlier play a large role in disturbing the plasma. Obviously, evaporated or sputtered probe material may enter the plasma resulting in large changes of n_e or T_e and resulting in global modification of confinement or even major disruption. Sputtering or evaporation may change the probe dimensions, and thus the effective collection areas, in unknown ways. Ion recycling on the probe itself may change the nature of the plasma in the measured region. This is a problem at high densities where re-ionization of ions neutralized at the probe can increase the local density and reduce the temperature. The effect is also likely to increase with probe size. Similar effects occur at the limiter and divertor target plate so the problem is really one of interpretation - relating the results obtained from the probe to the plasma conditions either close to or far from the limiter surface.

On a less dramatic scale, changes in the surface conditions of an electrical probe may lead to varying secondary electron emission, ion particle and energy reflection coefficients, or contact potentials, rendering the analysis difficult. The bombardment of electrical probes by impurities or metastable atoms also complicates the analysis since the secondary electron emission coefficient can be significantly changed. Overheating of the probe can drive it into thermionic emission where the above theory does not apply. Lastly, inherent fluctuations of n_e and/or T_e or T_i can be quite large in fusion plasmas. Such fluctuations are of fundamental physical importance and have been the object of recent studies using probes[39,40]. However, such fluctuations make the simple reduction of data described above quite uncertain. In particular, accurate determination of T_e can become very difficult.

4. MEASUREMENT OF ENERGY DISTRIBUTION

For the techniques described so far it is necessary to assume that the ion and electron energy distributions are Maxwellian. This is by no means certain as high energy components are known to occur under some conditions e.g. runaway electrons at low densities and high energy ions due to neutral injection. As mentioned earlier the comparison of measured power to ion saturation current and electron temperature, that is, a determination of the heat-flux transmission coefficient can indicate the presence of such fast components. In order to determine the identity of such components it is necessary to have some sort of energy analysis. A number of systems have been tried, including retarding field analyzers[41,42,43] and the ExB analyzer[44,45] but none have been widely used in tokamaks.

A problem common to all such analyzers is the proper design of the extraction and retarding field elements[46]. The particle trajectories, determined by the electric fields sampled on passing through the analyzer apertures may be subjected to unwanted divergence or focussing. The measured energy distribution functions can be distorted by defocussing effects such as field penetration[47], by space charge[48], or other geometric effects particular to the analyzer. Accurate description of the behaviour of such systems may require considerable computational modelling.

Complication also arises in using such devices in very strong magnetic fields wherein the alignment is critical. A misalignment of a few degrees to the total field may have serious consequences in some types of energy analyzers. This can lead to problems in mapping radial profiles in certain tokamak discharges if the magnetic field angle changes significantly over the region of interest.

4.1 Retarding Field Analyzers

The well known retarding field analyzer[49] is shown schematically in Fig. 9a. Ions or electrons can be analyzed by retardation in the field between grids. By sweeping the retarding field an integral distribution of ions above a given energy can be obtained. The differential spectrum can be obtained either computationally or electronically; one technique is to use a low amplitude high frequency sweep while simultaneously changing the retarding voltage[50]. While the retarding field analyzer is simple to use for monoenergetic beams problems arise in magnetized plasmas. It is first necessary to separate ions and electrons. If slits or grid meshes of size comparable to the Debye length, λ_D, are used then a sheath is set up and the electron flow into the analyzer is reduced to the value of the ion flow. However such fine grids will withstand only low incident power. A further

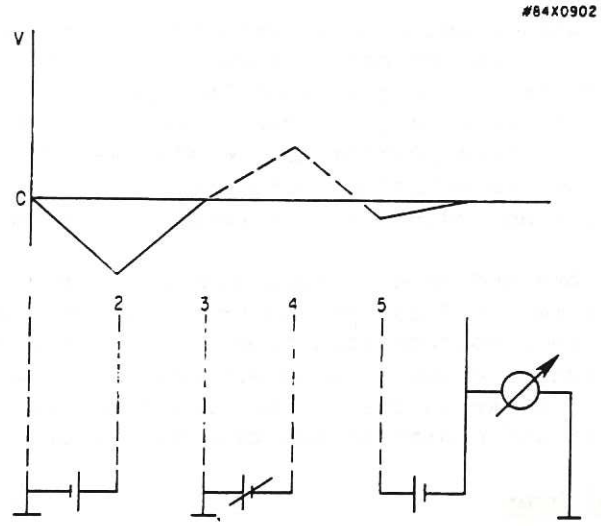

Fig. 9a Schematic of retarding field analyser (R.F.A.) particle energy analysis. By scanning grid 4 potential an integral energy distribution is obtained. By reversing polarity either ions or electrons can be analysed.

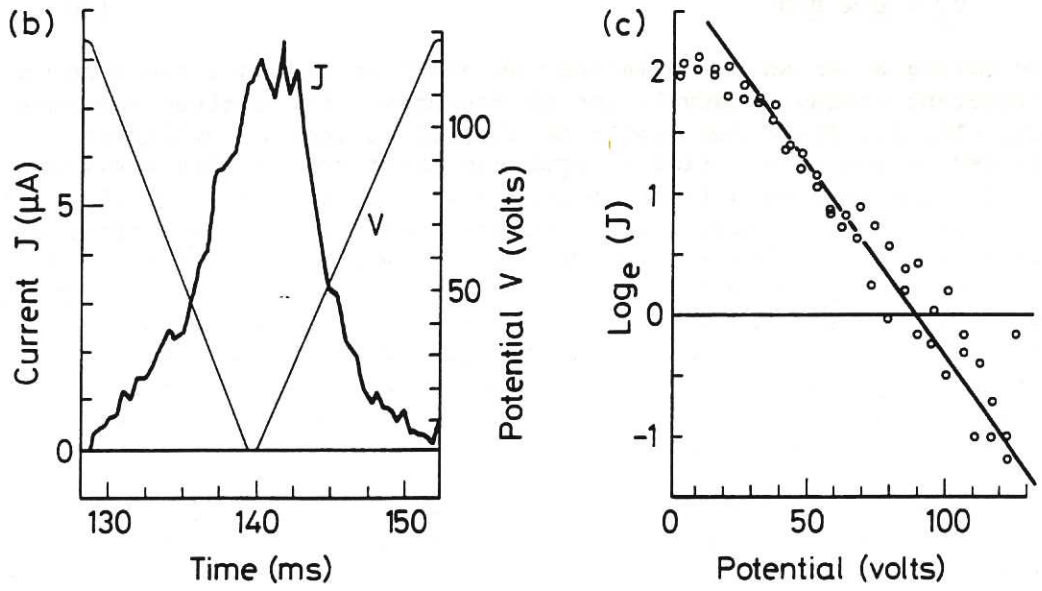

Fig. 9b An integral distribution from a retarding field analyser resulting from the voltage scan shown, Taken during an ohmically heated discharge in the DITE tokamak[45].

Fig. 9c A logarithmic plot of the ion current from 9b indicating a sheath potential of ~ 20 eV and an ion temperature of 32 eV.

problem is that when using a small grid mesh or narrow slit the effect of finite ion larmor radius must be taken into consideration. The thickness of the grid must be kept small compared with the hole size in order to prevent the attenuation of the ions with transverse energy. This problem can be alleviated to some extent by calculating the transmission factors of a given geometry as a function of energy and using this to correct experimental data.

Results[45] obtained in a tokamak boundary during ohmic discharges are shown in figs. 9b and 9c. Fig. 9b shows the raw data obtained with a voltage scan from + 120 to - 5 volts. The integral distribution drawn on a logarithmic scale in fig. 9c indicates the acceleration due to the sheath potential and a Maxwellian distribution with an ion temperature of 32 eV.

4.2 The ExB Analyzer

The ExB analyzer has been developed by Staib[44]. The ions enter the analyzer through a small hole or slit. An electric field E is applied at right angles to the existing magnetic confinement field B (Fig. 10a) The ions then have a drift velocity v_D in the ExB direction independent of their charge and mass:

$$V_D = \underset{\sim}{E} \times \underset{\sim}{B}/B^2 \qquad (26)$$

By having a series of collectors as shown in Fig. 10a the ions in different energy intervals can be detected. For a given geometry the electric field can easily be altered to look at different ranges of energies. Similar problems exist for the ExB analyzers as for the retarding field analyzers with regard to power flux and ion transmission through the defining hole. In addition there can be a greater problem with space charge. When the electrons are removed the space charge of the ions will create an electric field which may be significant compared with the applied field. This additional field may cause spreading of the ions which can make the measured energy distribution appear to be broader than it is. This effect will determine an upper limit to the plasma density which can be measured.

Despite these problems ExB analyzers have been used successfully in tokamak plasmas. By using a slit size of 30 μm, plasmas with density up to 5×10^{18} m^{-3} have been analyzed[45]. Ion temperatures obtained with an ExB analyzer compared with a retarding field analyzer are shown in fig. 10b. Good agreement has been obtained. A characteristic increase in ion temperature when the gas feed is turned off is illustrated. The almost continuous measurement of T_i obtained with the ExB analyzer is a valuable feature of this device.

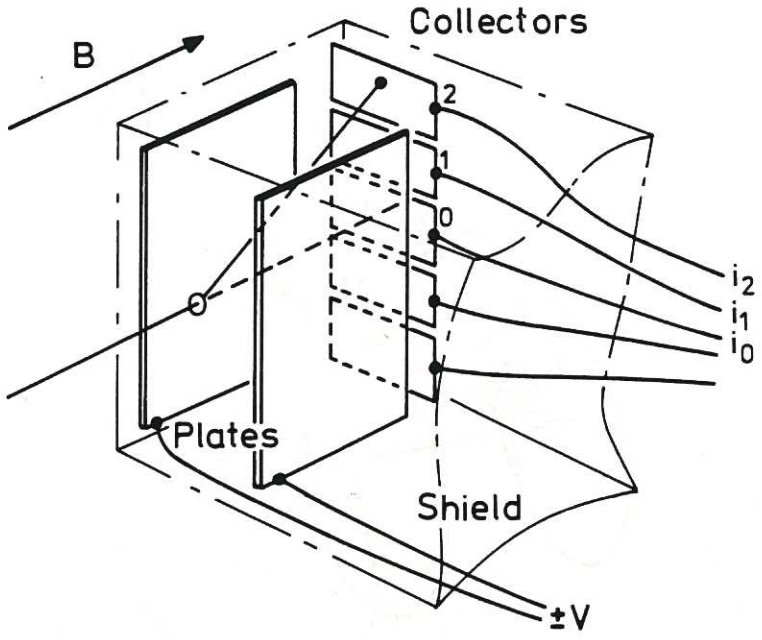

Fig.10a Schematic of an ExB analyser showing the electric field plates at potential ± V and five collectors.

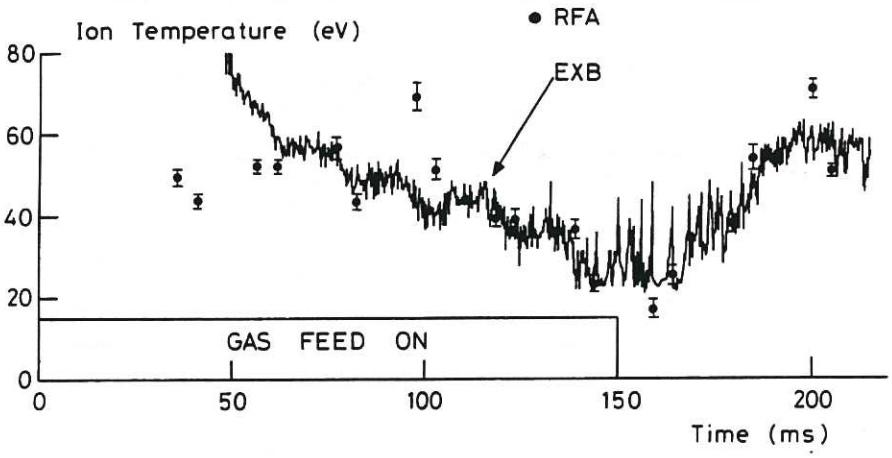

Fig.10b Comparison of results with an ExB analyser and a retarding field analyser (R.F.A.) taken in the same discharge on the DITE tokamak[45].

#83X0778

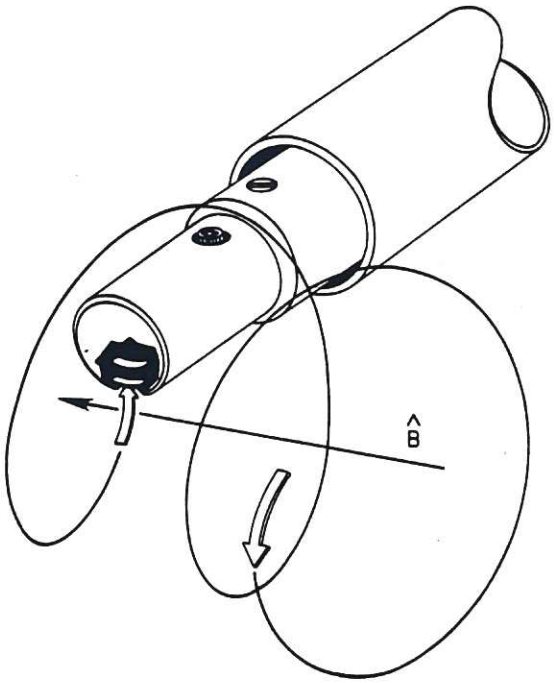

Fig.11a Rotating bolometer (heat flux) probe. The active elements are hidden behind an aperture in the cap. When the detectors are at a large angle with respect to the magnetic field only ions with large gyroradii are admitted.

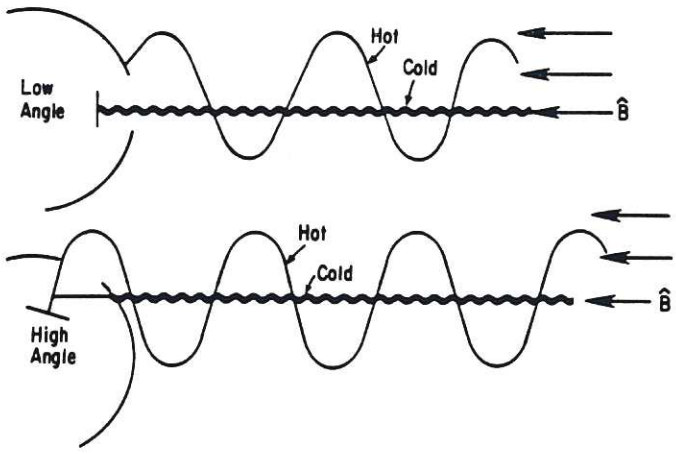

Fig.11b Effect of filtering action on fast and slow ions as the bolometer is rotated.

4.3 Rotating Calorimeter

Another energy discriminating electrical probe is the rotating calorimeter (or heat flux) probe developed for use on PLT, PDX, and TFTR[51]. It is based on the measurement of heat flux as described in section 3.5. Fig. 11a shows a schematic of the device. It consists of two calorimeter plates with thermocouples attached which are located relatively far behind apertures in a cylindrical carbon housing. The filtering action of the aperture is similar to that described for the collector-aperture probes which are discussed in section 5.2. Fig. 11b shows schematically how the filtering action can be employed to discriminate fast ions from slow ions or electrons.

To extract the actual velocity space distributions associated with a fast ion component is rather complicated. At present this is done via Monte Carlo calculations. Initial distributions of ion velocities are assumed and the anticipated distributions of heat flux vs. probe angle relative to the magnetic field are calculated. The fundamental parameters of the problem are aperture size relative to the ion gyroradius and the ratio of $v_\perp/v_\parallel$. The resulting angular distributions have a rather complicated behaviour in general. However, when the gyroradius

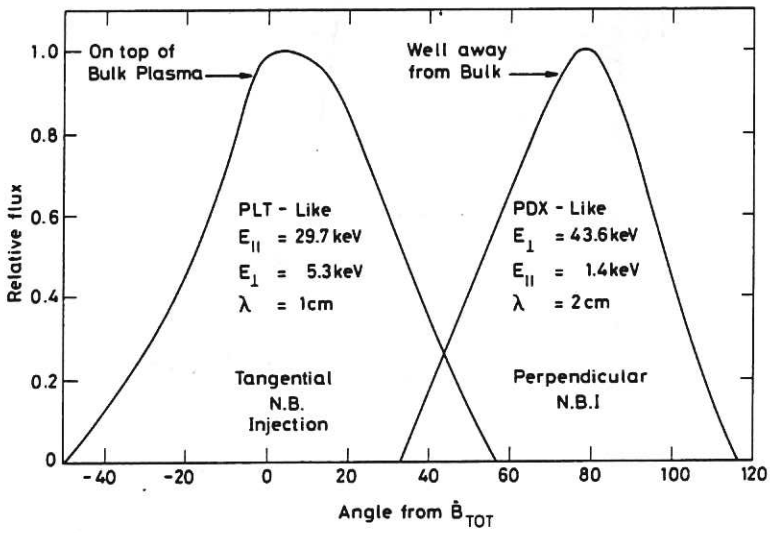

Fig. 12 The calculated distribution of fast ions at the outer midplane of PLT and PDX due to prompt losses of injected neutrals.

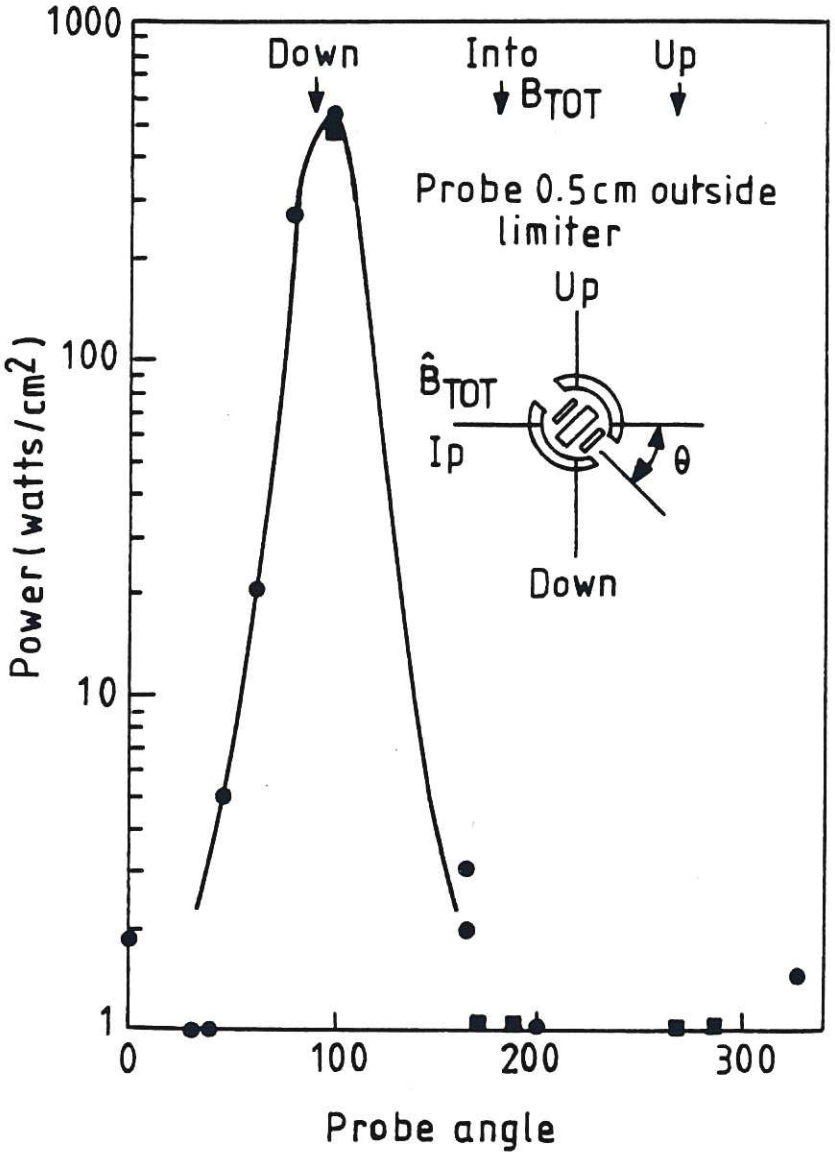

Fig. 13 Measurements of the angular variation of heat flux at the midplane of PDX during 4.2 MW NBI, B_T = 1.2 T, $\bar{n}_e \sim 3 \times 10^{18}$ m^{-3}, I_p = 250 kA.

is very much larger than the aperture size the resulting angular distribution is simply that associated with a plane parallel flux (zero gyroradius) shifted to a position such that $\Phi_{max} = \tan^{-1} V_\perp/V_\parallel$. Fig. 12 shows results anticipated for distributions of ions which would result at the outer midplane of PLT and PDX in the event of prompt loss during neutral beam injection. The two cases are very easily distinguished. Fig. 13 shows data taken during 4.2 MW neutral beam injection on PDX. The peak at $\sim 81^\circ$ from B_T indicates the occurrence of prompt beam particle loss.

4.4 Larmor Radius Techniques

There are a number of different methods of obtaining information on the energy distribution from the ion larmor radius[52,53,54,55]. One ingenious technique is the Katsumato

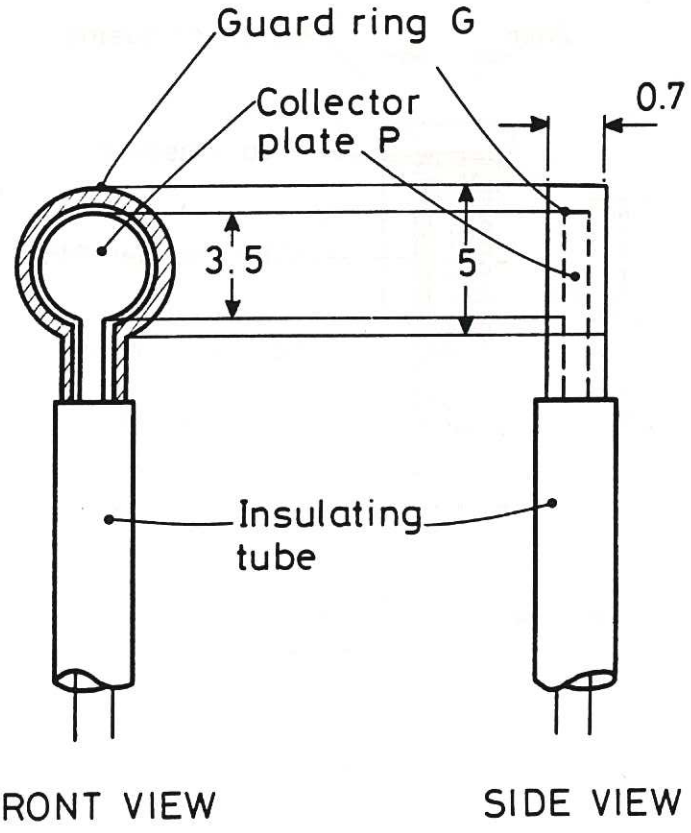

Fig. 14 The Katsumato probe. A collector plate P is mounted with its plane parallel to the magnetic field. A guard ring G shields P from electrons. Dimensions in mm.

probe[55] which is shown schematically in fig. 14. Because of their small larmor radius electrons are prevented from reaching a centre disc collector when it is aligned with the magnetic field. Ions with their larger radius can reach it. A retarding potential characteristic is taken using the disc electrode and from this ion energy distributions have been estimated. However, there has been no treatment of the effect of space charge due to the separation of ions and electrons and it is unlikely to work satisfactorily except at low densities. Results have been presented for the DIVA[56] and TCA[57] tokamaks.

A versatile energy analyzer for electron distributions has been described by Arion and Ellis[52]. The device is based on the absorption of ions by small cylindrical channels as plasma traverses their length, thus the charge separation physics differs from retarding field in beneficial ways that allow the device to be made quite small. Stenzel et al[53] have constructed a similar

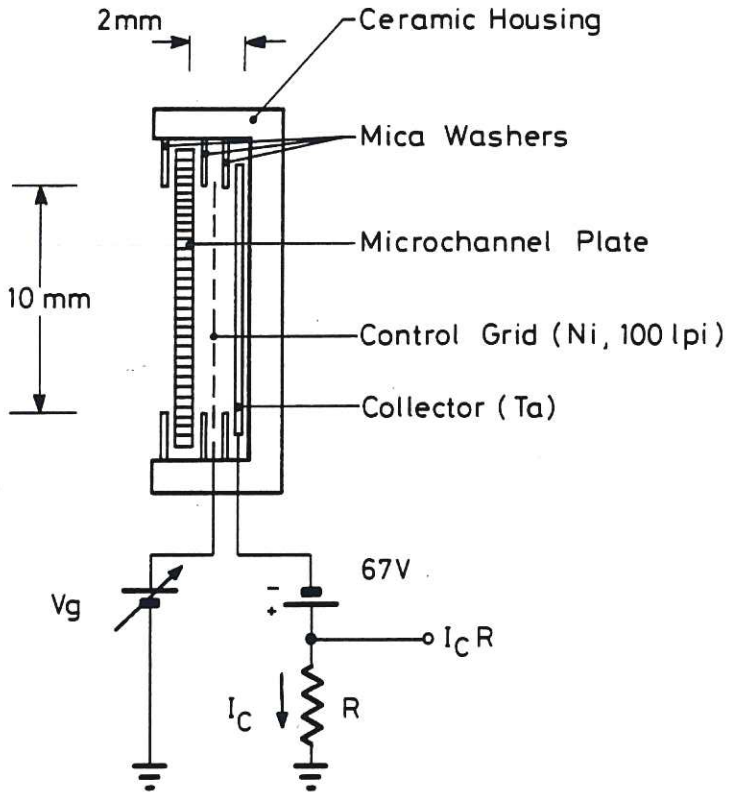

Fig. 15 A microchannel energy analyser. Ions are separated out because of their large larmor radius and the voltage on a simple grid is scanned to obtain the electron energy distribution.

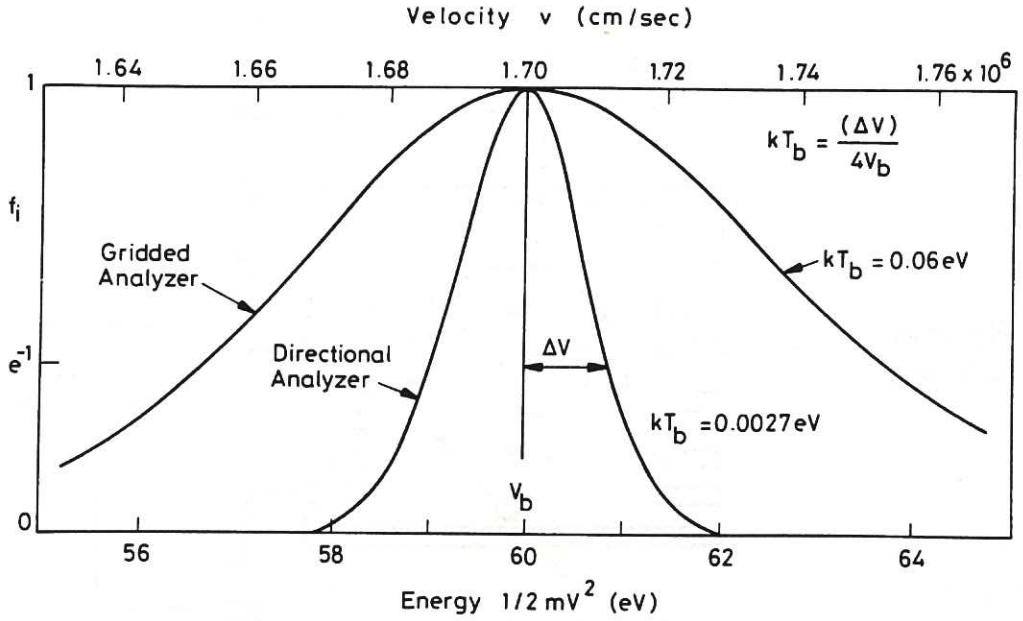

Fig. 16 Comparison of results from a microchannel energy analyser with a conventional retarding field analyser.

device wherein the channels are provided by a commercial microchannel plate as shown in Fig. 15. Fig. 16 compares the results of this analyzer to a conventional gridded analyzer immersed in a 60 eV beam generated in a double plasma device. Energetic electron tails are also easily measured in plasmas of densities up to 2 x 10^{12} cm^{-3}.

4.5 In Situ Mass Spectrometers

The main drawback of the electrical probes we have described so far is that they are insensitive to the ion mass. In principle the presence of the magnetic field should allow an electrical configuration which will provide mass analysis. Of the many configurations possible the presence of the strong magnetic field throughout the probe appears to restrict us to three possibilities. These are shown in figs. 17, 18 and 19 and have all been quite widely used in other mass spectrometric applications[58]. Application to plasma analysis introduces many of the same sampling problems we have discussed for the energy analysers. However if we assume these problems can be overcome or corrected we take a plasma sample through a small floating aperture. The ion beam emerging from the aperture has then an electric field applied in one of the following ways.

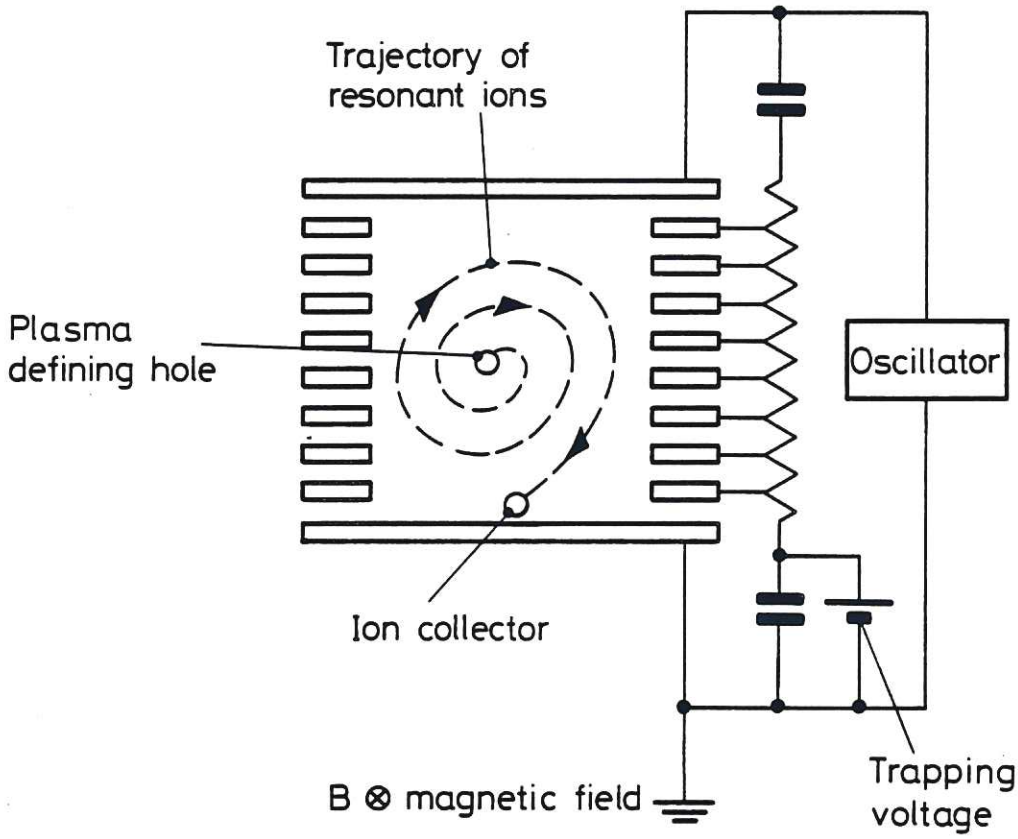

Fig. 17 Schematic of the omegatron mass spectrometer. Resonance ions are accelerated by the rf field until they strike the collector.

(i) The first approach fig. 17, is the omegatron. This has been used conventionally both for residual gas analyzers and for accurate mass determination. An rf field is applied as in a cyclotron. The frequency of the rf is swept and when it is resonant with the ion cyclotron frequency the ion is accelerated in a spiral. An ion collector near the rf electrodes allows the resonance peak to be detected. Relatively low potentials are required and problems occur when used as a residual gas analyzer with charge build up on electrodes. No application to plasma analysis has been published.

(ii) The second approach is to use the 180° sector focussing magnetic field. In order to increase their larmor radius the ions are accelerated in a strong electric field at right angles to the magnetic field, fig. 18. The ion then passes through a slit into a region with zero electric field and describes a circular orbit until it reaches a detector. The electric field is swept and ions

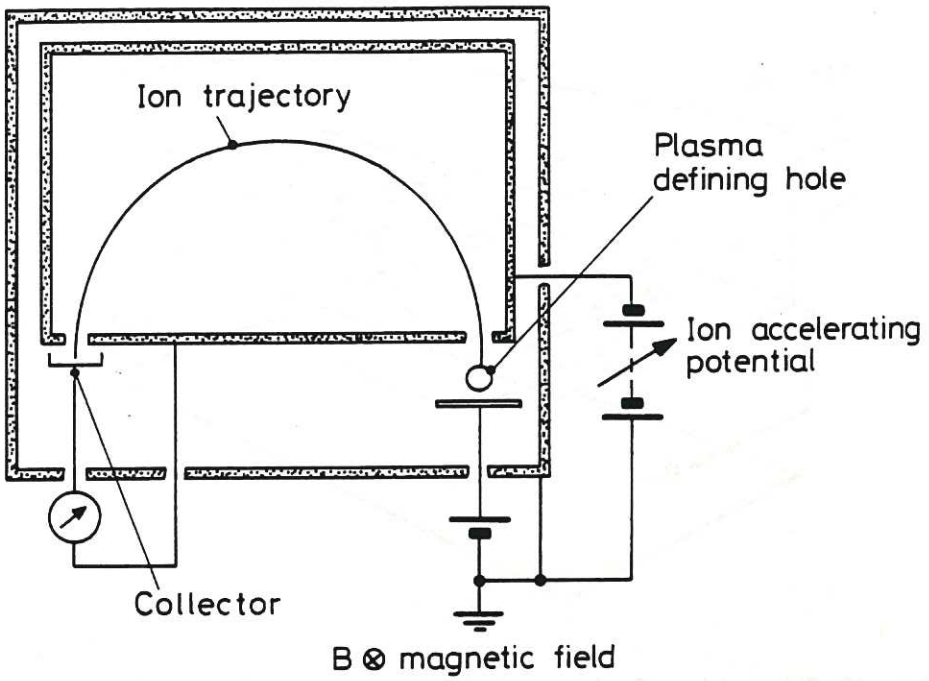

Fig. 18 Schematic of the 180° sector field mass spectrometer.

of increasing mass are successively focussed on the collector slit. The technique was successfully used for impurity analysis in the divertor of the C stellerator[59] and more recently has been used in other relatively low field plasma devices[60]. No successful application to a tokamak has been reported. Problems arise with the focussing and extraction of the ions in the electric field region. A large parallel velocity results in the ions continuing to travel along the field while describing the circular transverse orbit. The time to reach the collector slit in the plane normal to B must be less than the time taken to travel the length of the slit parallel to B. In principle this distance should allow the parallel velocity to be measured. However the problems which arise from the initial velocity of the ion causing chromatic aberration are likely to cause serious degradation in resolution. This arrangement of fields provides first order focussing in one direction only.

(iii) The cycloidal mass spectrometer has an arrangement of uniform crossed electric and magnetic fields which in principle provides both directional and energy focussing, fig. 19. The problems of ion sampling and acceleration are similar to those described for the other devices. In addition it is important to

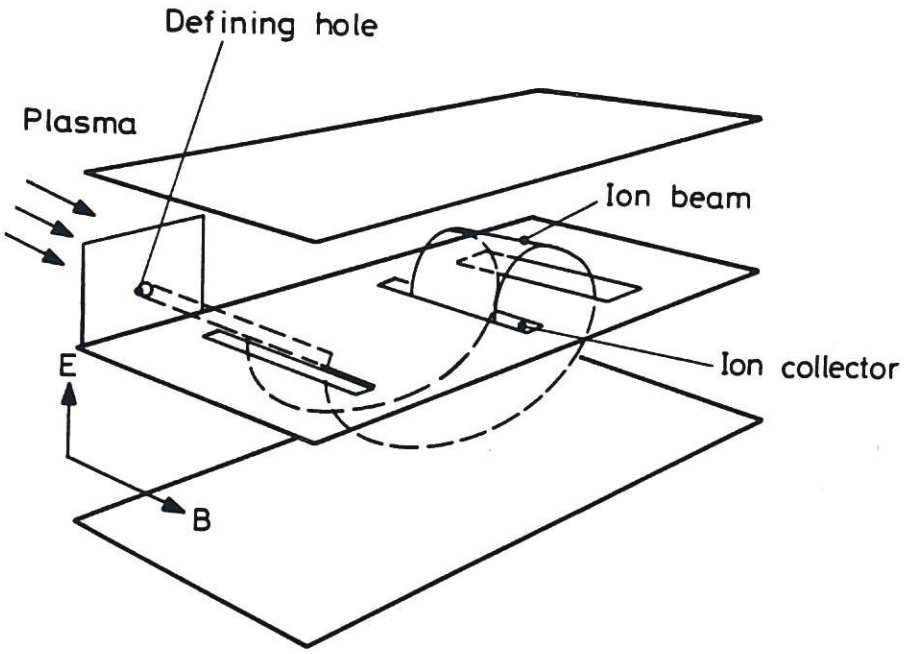

Fig. 19 Schematic of the cycloidal mass spectrometer. Ions are subjected to a uniform electric and magnetic field and perform a cycloidal path to the collector.

have a uniform electric field. The condition for focussing is

$$\frac{m}{e} = \frac{dB^2}{2\pi E} \qquad (27)$$

where d is the distance between the slits, and E and B are the electric and magnetic fields. There is no known use of this arrangement for plasma analysis.

5. FLUX MEASUREMENTS USING SURFACE ANALYSIS

5.1 Theory

We have already discussed the flux measured by electrical probes and how this can be interpreted to give the ion density. However, the analysis assumes that the probe is non-perturbing. Generally speaking collector probes are larger than electrical probes and must therefore be considered perturbing. In a magnetic field flow is predominantly along field lines and the presence of a probe is therefore perturbing in the sense that it adsorbs the incident flux. The flow to the probe in this circumstance is

replenished by cross field diffusion. It can readily be shown[61] that for a rectangular flux tube connecting with the probe, in the absence of source terms within the flux tube,

$$\Gamma_{\perp} A_{\perp} + \Gamma_{\parallel} A_{\parallel} = 0, \tag{28}$$

where $\Gamma_{\perp}$ and $\Gamma_{\parallel}$ are the fluxes perpendicular and parallel to the field and $A_{\parallel}$ and $A_{\perp}$ are the areas of the cross section and the side of the flux tube. In what follows it is assumed that ionization is negligible within the flux tube defined by the probe. Ionization is negligible whenever the ionization rate $\langle \sigma_{eii} v_e \rangle n_o n_e$. V is small compared to the probe current, where σ_{eii} is the electron impact ionization cross-section, n_o is the neutral density, n_e is the electron density, and V is the volume of the flux tube. When this condition does not apply one must add the ionization rate as a volume source term in the conservation equations for particles (equation 28 above) and momentum (see chapter by Stangeby). The parallel ion and electron flux Γ are given in general for the collisional case by the equation

$$\Gamma_{\parallel} = - D_{\parallel} \left[\frac{dn}{dx} + n\mu_{\parallel} E\right] \tag{29}$$

where $D_{\parallel}$ and $\mu_{\parallel}$ are the diffusion coefficients and mobilities along B. An analysis of the cross field and parallel fluxes leads to an expression for the electron saturation flux,[62,63]

$$\Gamma_{\parallel,e} = 1/4\, n_e c_e \left(\frac{r}{1 + r}\right) \tag{30}$$

where

$$r = \frac{16}{\pi} \frac{\lambda\sqrt{\alpha}(1 + T_i/T_e)}{d}, \tag{31}$$

$\alpha = D_{\perp}/D_{\parallel}$, d is the probe size and λ is the electron mean free path. Equation (30) is a modified form of equation (8). For strong magnetic fields $r << 1$ the electron saturation current is reduced by a large factor compared with the value in zero field. This reduction can affect the voltage range over which $\ell n(I + I_{sat})$ is proportional to V and hence the parameter range over which T_e should be calculated.

We now consider the ion flux, following the analysis presented by Cohen[61]. The potential variation along the flux tube towards the probe is shown in Fig. 20. With the probe at large negative potential the ions get continuously accelerated and the flux is given by the ion saturation current as discussed in section 3.1. For a probe at a large positive potential

$$V_p > (T_i/T_e)\, \ell n[(1 + r)/r] \tag{32}$$

the ion random flux is reduced by a simple Boltzmann factor

$$\Gamma_i = 1/4\ n_o\ c_s\ \exp\ (-\ eV_p/kT_i). \qquad (33)$$

For intermediate potentials the ions see a potential hill, V_H, between the undisturbed plasma and the probe. This hill can be thought of as due to the resistance of the plasma to the electron flow[61]. The ions are retarded as they approach it and their

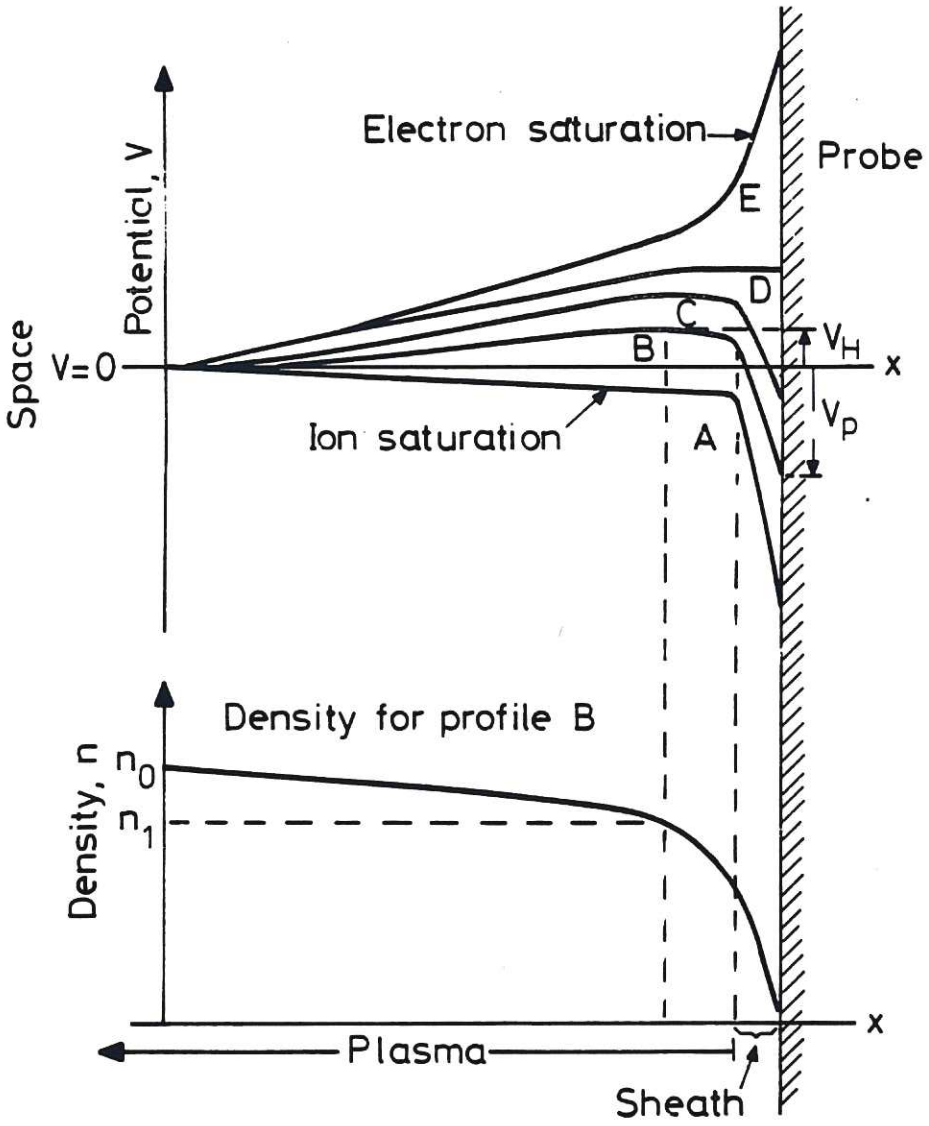

Fig.20 Potential and density variation along a flux tube as a function of distance from a probe surface. Potential distributions are shown for different applied probe potentials A to E.

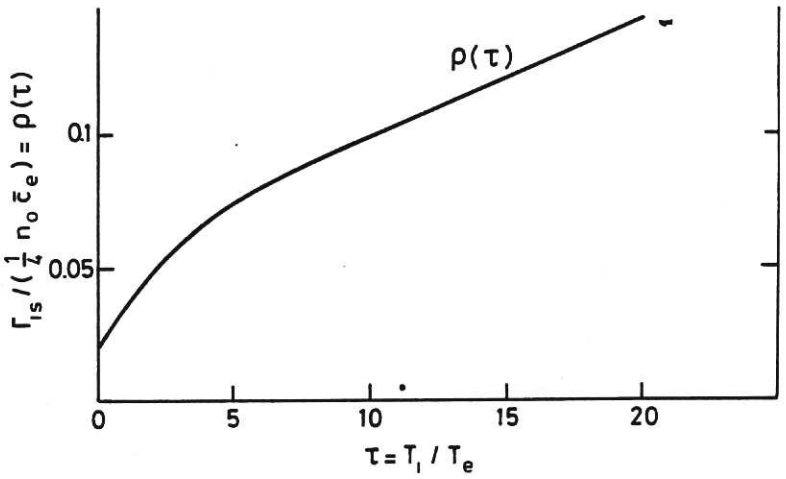

Fig. 21 Ratio of ion saturation current to electron saturation current as a function of the ratio T_i/T_e for the case of collisionless flow.

density is reduced to n_1 at the top of the hill

$$n_1 = n_o \exp (- V_H/kT_i). \tag{34}$$

The ion current flowing to the probe becomes

$$\Gamma_i = n_1 \left[\frac{k(T_e + T_i)}{m_i}\right]^{1/2}. \tag{35}$$

The value of n_1 depends on the collisionality of the plasma. For the case of collisionless ion flow it has been shown that[63]

$$\Gamma_i = \rho(T_i/T_e)\ 1/4\ n_o c_e \exp (- V_H/kT_i). \tag{36}$$

$\rho(T_i/T_e)$ is a complex function which is shown graphically for D^+ ions in Fig. 21 and c_e is the electron random velocity defined in section 3.1. In the ion saturation region the ion flux reduces to

$$\Gamma_i = \rho(T_i/T_e)\ 1/4\ n_o\ c_e \tag{37}$$

It is seen that the ion flux is quite a strong function of the T_i/T_e ratio. For D^+ $\rho(T_i/T_e)$ varies from 0.02 at $T_i = 0$ to ~ 0.1 at $T_i = 10\ T_e$. The general form of $\rho(T_i/T_e)$ can be deduced from the theory of Emmert et al.[64].

The question of the collisionality of the plasma has been

considered by Cohen[61]. The plasma is collisional if the ion-ion mean free path is short compared to the flux collection length, L. The situation is complicated depending on whether impurities are present or not. It has been concluded that in much of the region accessible to probes the plasma is sufficiently collisional to affect the parallel motion of H^+ ions and highly ionized impurities, e.g. O^{6+}. The flux tube length L is approximately given by

$$L = 0.5\ d(D_{\parallel}/D_{\perp})^{1/2} \tag{38}$$

and the ion-ion collisional time is given by[65]

$$\tau_{ii} = \frac{3\sqrt{m_i}(kT_i)^{3/2}}{4\sqrt{\pi}\ n\ \ell n\Lambda\ e^4}\ . \tag{39}$$

Where $\ell n\Lambda$ is the Coulomb logarithm. If we assume D^+ ions, $\ell n\Lambda$ = 10 and $D_{\perp} = 2.5 \times 10^{16}/n$ we obtain

$$nd < 1.1 \times 10^{12}\ T_i^{0.75}\ (T_i \text{ in eV})\ . \tag{40}$$

Thus for d = 1 cm, T_i = 10 eV we have $n_e \sim 10^{12}$ cm^{-3} as the upper limit that may be regarded as collisionless. The inclusion of other collisions (ion-neutral, ion-impurity, etc.) will further reduce the permitted density.

For operation with collection probes it is most convenient to maintain the probe at floating potential, both to simplify the interpretation and to minimize the heat flux to its surface.

5.2 Surface Collector Probes: Hydrogen Isotopes

The hydrogen isotope flux measurement by surface collection has been used on a number of tokmaks[66]. Like other surface techniques it has the advantage of allowing measurements to be made after the discharge and away from the electrical interference present during the discharge. It also has the advantage of allowing differentiation between various isotopes present. The disadvantage associated with these methods is a lack of real-time feedback to assist in tokamak operations or to guide the experiment in progress. Such a disadvantage is often serious.

The interaction of energetic particles with solid surfaces is reviewed in detail by Behrisch (these proceedings). The use of collector probes for edge plasma analysis requires interpretation of the implantation profiles which result from particle bombardment. We briefly sketch the physical principles involved in the development of the implantation profiles.

When an energetic ion or neutral atom strikes a solid it loses energy at an energy dependent rate. At high energies the predominant loss is via interaction with the lattice electrons while at lower energy, loss of energy occurs via collisions with the lattice nuclei, the ions undergoing scattering. The particles of an incident beam come to rest at a distribution of depths. The depth profiles are accurately calculable for amorphous solids by Monte Carlo codes[67] and are fairly well represented by gaussian profiles modified to account for reflection loss at the front surface[68]. The 1st moment (mean) of depth profiles so constructed is known as the "mean projected range" and the 2nd moment (variance squared) is called the "depth straggling". A knowledge of the depth profile can sometimes be related to the energy distribution of the incident particles for a given target if it is assumed that the particles are trapped at their stopping point in the lattice and do not subsequently diffuse. Thus only materials, such as carbon, silicon and beryllium which have very low diffusion coefficients for hydrogen can be used. Carbon and beryllium also have low atomic numbers and thus the fraction of the incident hydrogen flux which is backscattered is low and the sensitivity of the method is enhanced. The most commonly used carbon samples for such probes are carbon ribbon (PAPYEX or POCO), amorphous carbon films, and compression annealed pyrolytic carbon.

As the incident ions are trapped in the solid the concentration increases linearly. Eventually the concentration reaches a saturation level, first at the peak of the range profile and then gradually the saturation region expands, see fig. 22. The mechanism responsible for saturation is not well understood but the saturation level has been measured to be 0.44 hydrogen atoms/carbon atom[69] at room temperature. As the range of hydrogen ions is roughly proportional to energy the areal density (atoms m^{-2}) at which the surface is saturated is dependant on the incident ion energy. Thus by measuring the trapped fluence as a function of incident fluence the incident flux can be obtained from the initial linear part of the curve and the energy can be obtained from the saturation level.

In order to obtain the incident flux from such measurements it is necessary to know the form of the incident ion energy distribution since this determines the number of incident ions which are backscattered. If the energy distribution form is known, e.g. Maxwellian or monoenergetic, then there are a number of detailed models which can be applied. Wampler et al.[70], have done a careful calibration of these models with experimental data using ion beams to implant samples. They have shown that by taking a series of exposures of samples to different fluences whose ratio is known but whose absolute value is not known, the value of incident flux and the ion energy or temperature (depending on the assumption about the energy distribution) can be derived. In principle this

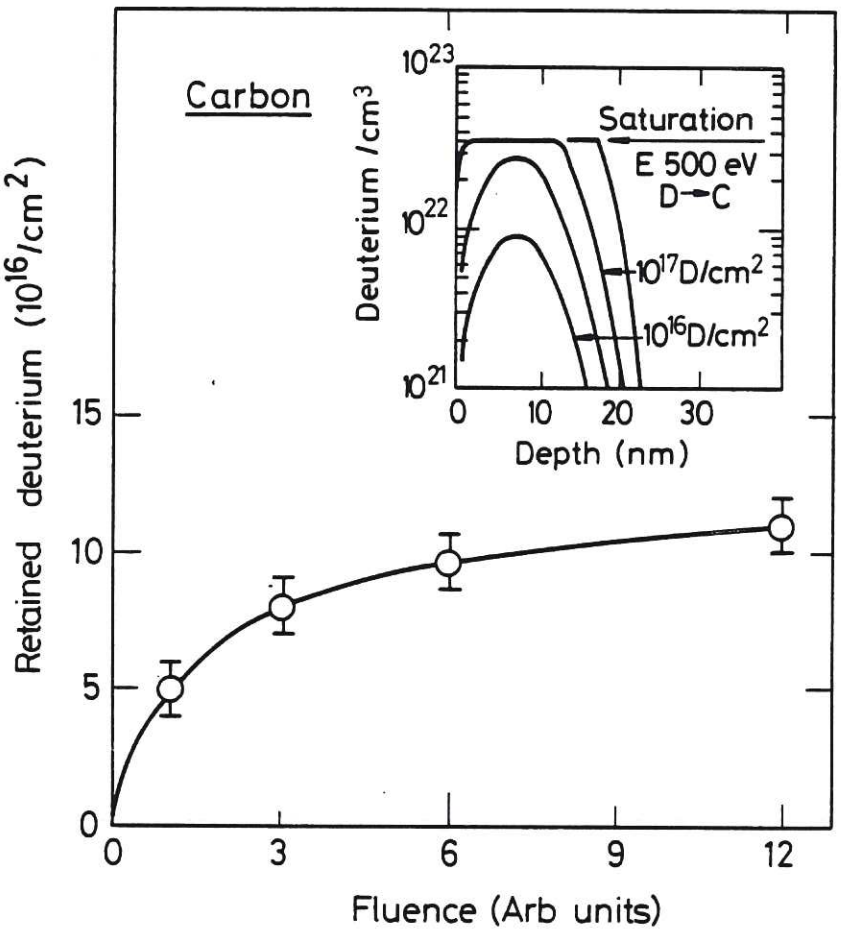

Fig.22 Experimental measurements in HT of deuterium retained in a carbon probe as a function of incident fluence. The insert shows schematically the depth distribution in the solid illustrating how the retained deuterium increases at first linearly and then saturates.

technique is quite easy to apply since samples can be exposed to different numbers of discharges. In practice, there are serious problems with the method. The integration of collected flux over time in the discharge is highly undesirable. Time-resolved measurements show that the flux and particle energy change dramatically over the course of a tokamak discharge often showing large start-up and termination flux transients.[71,72,73] These parameters vary a great deal during auxiliary heating as well. Thus a time averaged value may be of little value in interpreting the physics of the edge plasma. There has been a large discrepancy between the flux measured by collector probes and that measured by Langmuir probes when these have been compared[74]. This

could be the result of such time averaging or of the collector probes losing a large fraction of the low energy component of the plasma flux.

A variety of methods for measuring the areal density (atoms m^{-2}) is available. These methods include nuclear reactions[75], e.g. $^{1}H(^{15}N,\alpha\gamma)^{12}C$ and $^{2}H[^{3}He,p]^{4}He$, thermal desorption[76], forward nuclear scattering and Secondary Ion Mass Spectrometry (SIMS). Thermal desorption is relatively simple, it is sensitive and can often be carried out "in situ". By using a mass spectrometer all isotopic species can be detected. The nuclear techniques require the use of an accelerator and therefore normally require the collectors to be removed from the tokamak. The hydrogen nuclear reactions also require high energies (~ 5 MeV) but the $^{2}H[^{3}He,p]^{4}He$ reaction is very simple, and has good sensitivity. Ross and co-workers[77] have recently developed a low energy (350 keV) helium elastic recoil apparatus for H^{+} and/or D^{+} depth profiles with a resolution of ~ 5 nm and an ultimate sensitivity of 0.1 atomic %. Energy analysis of scattered products or nuclear resonance methods permit these species to be depth-profiled to an accuracy of ~ 10 nm, sufficient for many probe applications e.g. fast neutrals lost during neutral injection heating[78] or minority ion cyclotron resonance heating[79]. SIMS permits more accurate depth profile determination ($\lesssim$ 20 Å) and this is more useful for low energy plasma implants (T_i ~ 50 eV) frequently associated with the scrape-off layer. The use of two or more of these techniques on the same samples is often valuable. Fig. 23 shows nuclear reaction analysis of the retained deuterium during PDX neutral beam injection, further analyzed by SIMS to obtain depth profiles at various times indicated on the nuclear reaction analysis, fig. 24. The deep (E ~ 47 keV) beam component is clearly evident. A similar combination of SIMS and ERD is shown for beam-heated PLT discharges in fig. 25. In both cases the non-quantitative SIMS profiles were supplemented by absolute flux measurements of the other method.

Another method for determining ion energy with surface collector probes takes advantage of the effect of finite larmor radius on transmission of ion through an aperture normal to the total magnetic field[80]. The details of the method depend on the specific geometry of the aperture as shown in fig. 26. When the aperture length is large enough to permit more than one full gyro-rotation of the particle as it traverses the opening the aperture is said to be thick. Otherwise it is said to be thin.

It is possible to use electrical collectors behind such apertures by examining the total transmission (collected current). Krawec[81] has given a detailed analysis of the problem for both thick and thin apertures and has presented a complete set of numerical calculations in terms of dimensionless parameters in

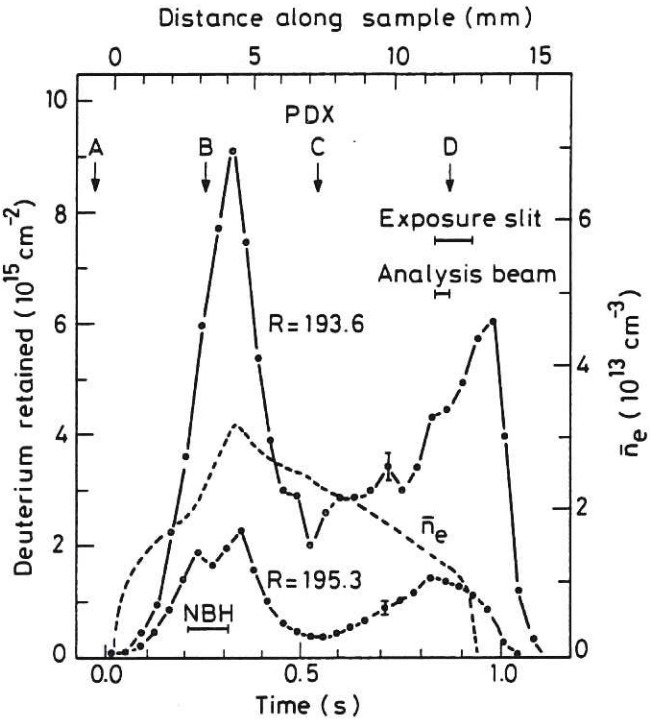

Fig. 23 The deuterium retained in two silicon probes as a function of time during a PDX discharge. The probes are at two different radii. The time when neutral beam heating (NBH) was applied is indicated. Depth profiles were measured at times indicated A,B,C,D.

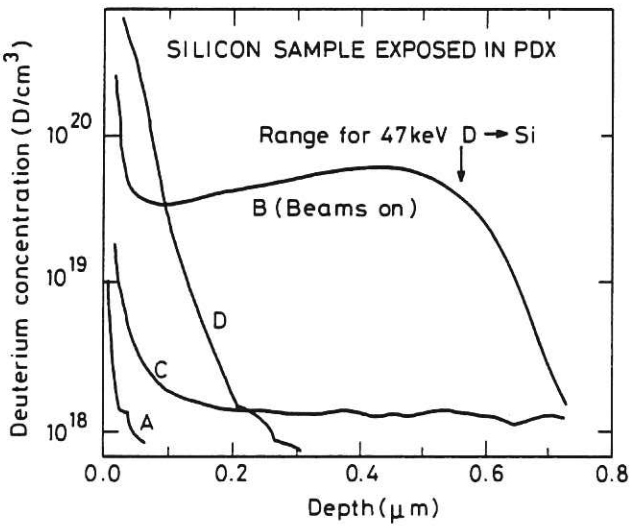

Fig. 24 The depth distribution of deuterium trapped in a silicon sample at various times during exposures in PDX as indicated from fig. 23.

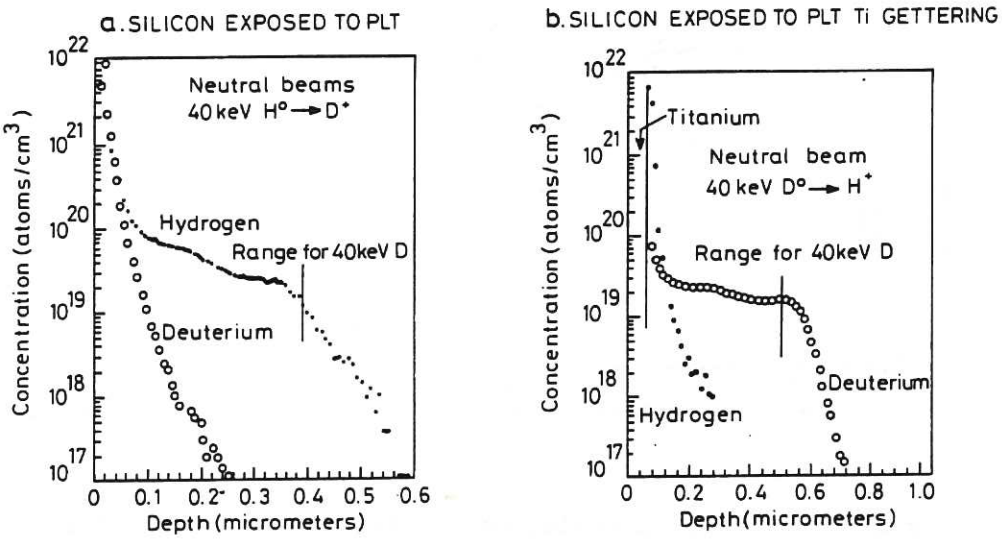

Fig. 25 (a) and (b) The depth distribution of H and D trapped in silicon during exposure in PLT determined by SIMS. The calculated range for normally incident 40 keV H(a) and D(b) ions are indicated.

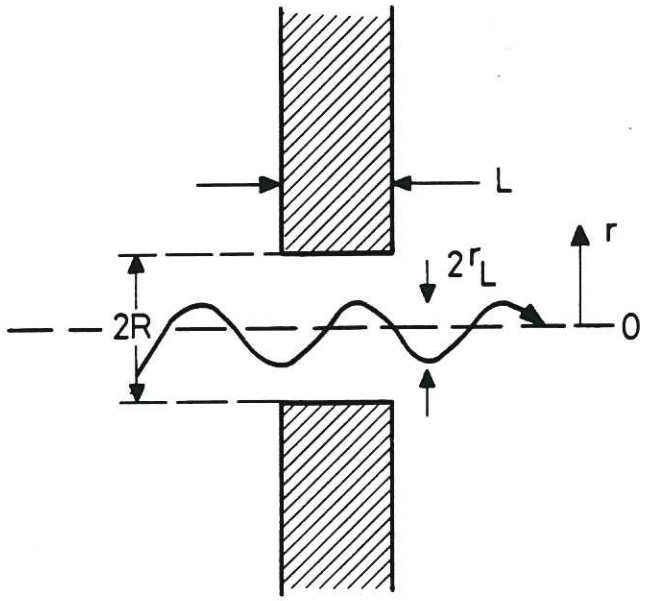

Fig. 26 Schematic of the transmission of ions of larmor radii r_L going through an aperture of thickness L and radius R.

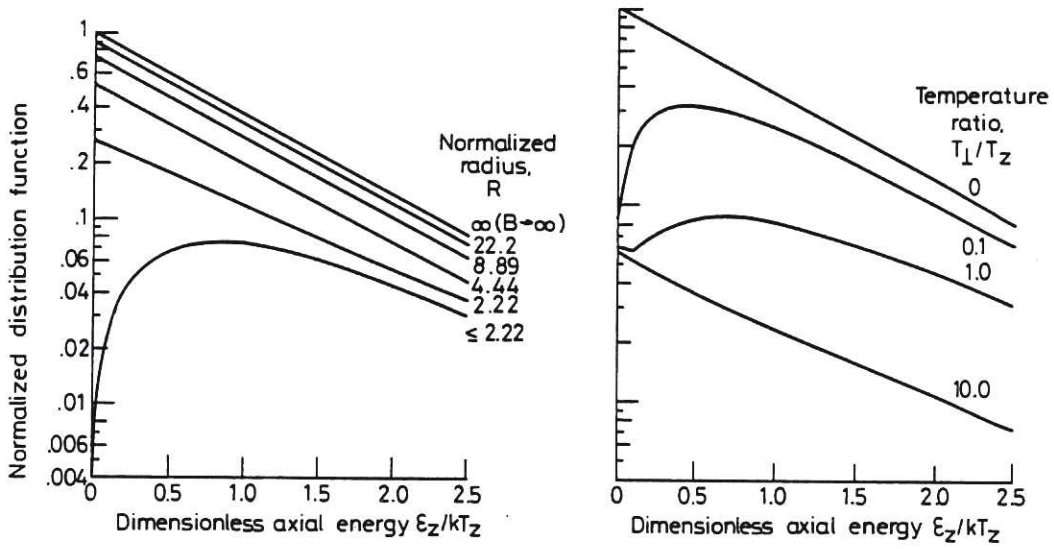

Fig.27 Results of calculations of the transmission of ions of larmor radius r through a hole of radius R in a plate of thickness L.

(a) Effect of varying the magnetic field for an L/R ratio 2.0 and a temperature ratio 1.0.

(b) Effect of varying the transverse to axial temperature ratio L/R and 2.0 normalized aperture radius 0.889.

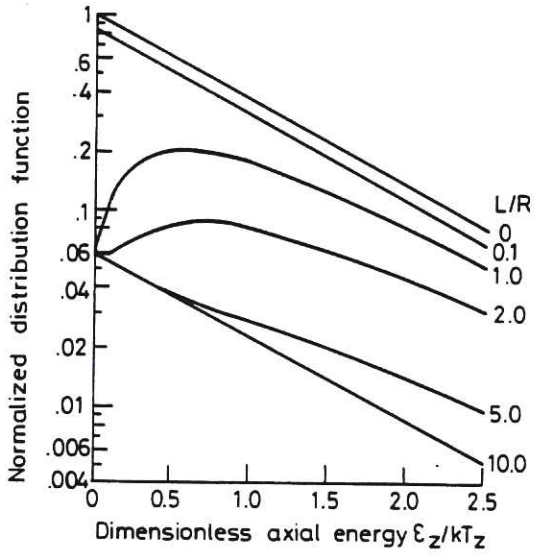

(c) Effect of varying the L/R ratio. Temperature ratio 1.0 normalized aperture radius 0.889.

the problem; examples are shown in fig. 27. On fusion devices such work has employed only sample collector surfaces for detection. Staudenmaier[80] and coworkers have considered the thick aperture case and derived an analytical expression for the transmission as a function of distance from the aperture centreline. An example of the expected behaviour of a 0.15 cm aperture in a 4T magnetic field is shown for the case of D^+ ions in fig. 28. The extraction of an ion temperature requires the assumption of an isotropic Maxwellian ion distribution. Such an assumption is likely to be untenable in many instances since sheath acceleration, plasma rotation, or auxiliary heating all may

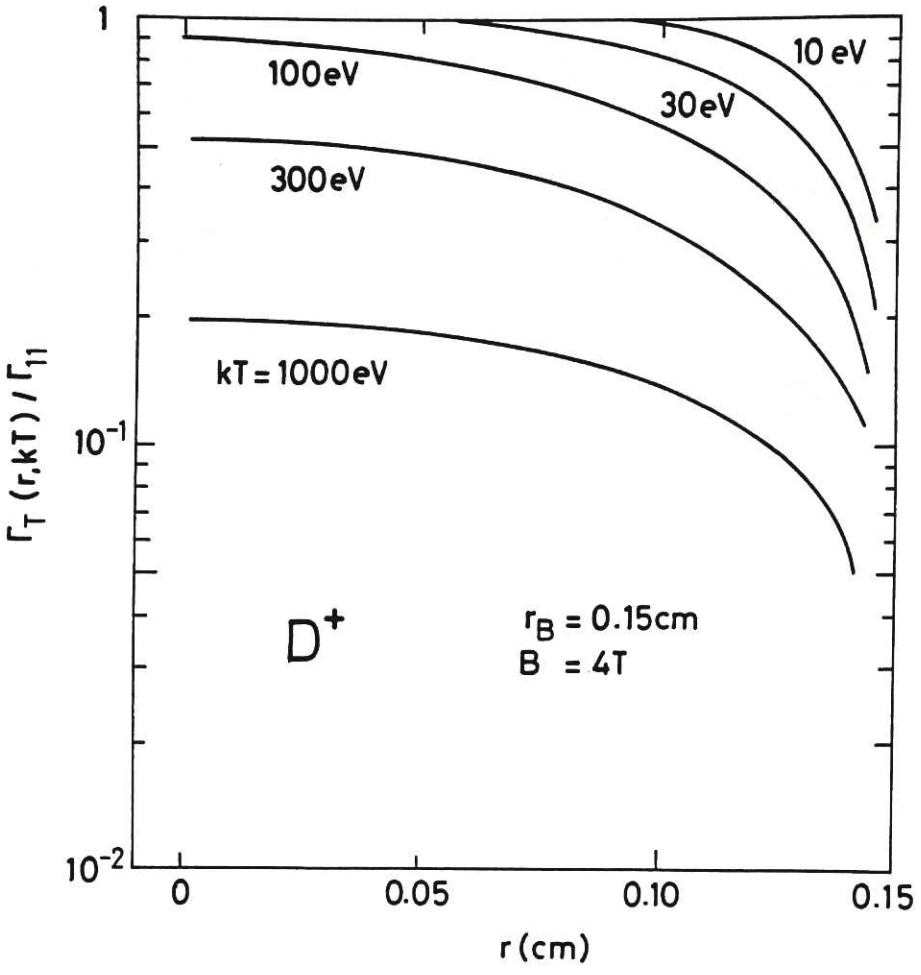

Fig.28 Calculated spatial distribution for deuterium ions of various temperatures between 10 eV and 1000 eV on a collector behind a hole of radius 1.5 mm in a toroidal field of 4 Tesla.

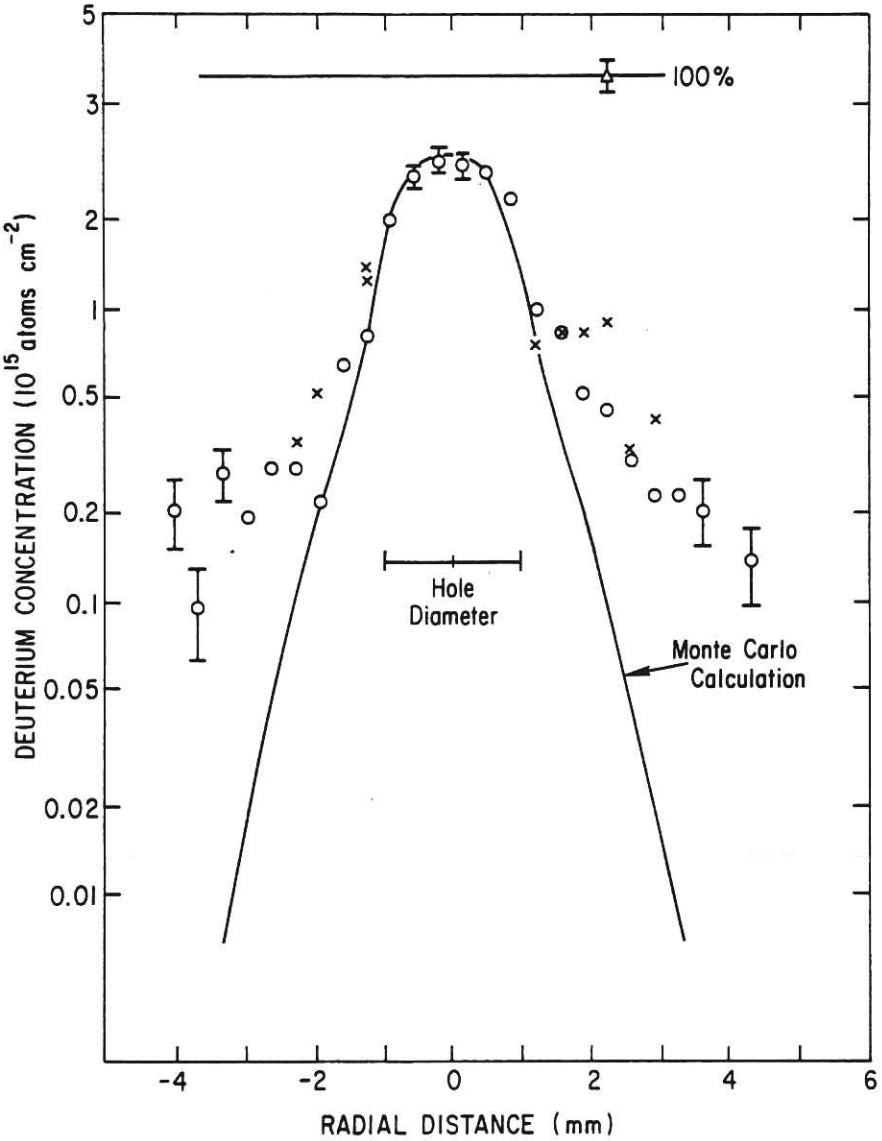

Fig. 29 Experimental measurements of the spatial distribution behind a hole of 2 mm diameter for deuterium ions in the DITE tokamak at a field of 2 Tesla. The Monte Carlo calculation is the distribution expected for ions of temperature 60 eV.

generate non-Maxwellian, anisotropic ion distributions. Zuhr et al. have accounted for non-Maxwellian distributions in their Monte-Carlo orbit calculations[82]. Their calculated results are in quite good agreement with the data. Less satisfactory agreement is seen in fig. 29 for D^+ from the DITE tokamak. Multiple ion reflection[83] may be a complication in this case.

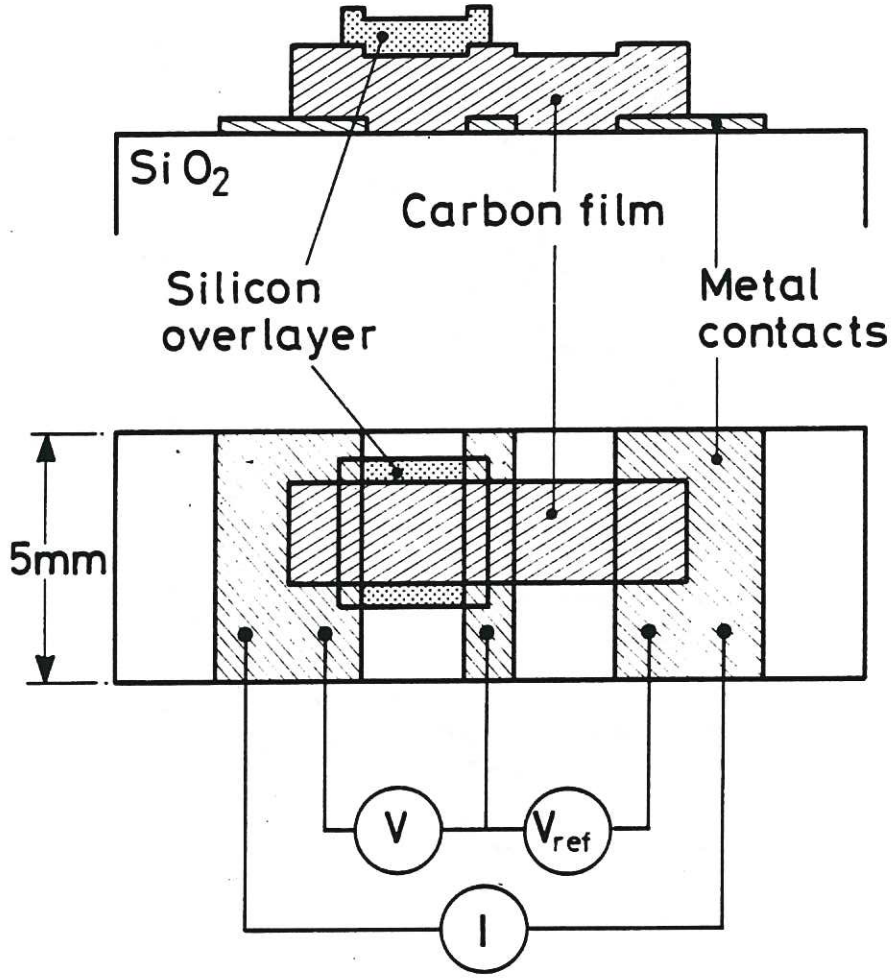

Fig. 30 Schematic of the carbon resistance probe.

5.3 Carbon Resistance Probe

A probe technique using a carbon thin film to measure ion energy has been developed by Wampler[84,85]. Since direct electrical measurements can be made in situ this technique should perhaps be included in section 3. However because it depends on surface modification due to ion bombardment it is more logical to include it with the other surface techniques. The active element is a thin film of carbon with a resistance which varies in a well-characterized manner as it is damaged by an incident particle flux. A schematic of the probe is shown in fig. 30 and the technique is similar to the standard 4-Point and Van der Pauw

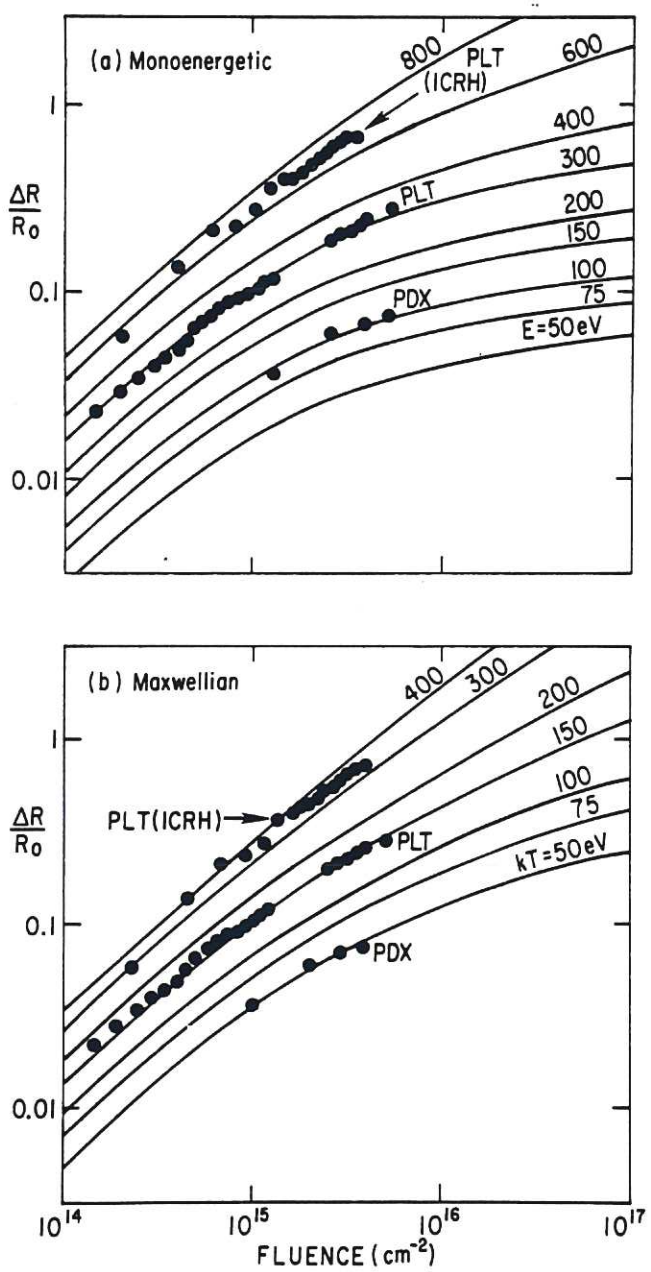

Fig. 31 Experimental results obtained using a carbon resistance probe in PLT and PDX compared with theoretical results obtained from ions of various energies. R_o is the resistance of the undamaged probe.

resistance diagnostic methods of ion-beam dose determination[86] in the semiconductor manufacturing industry.

The method relies on a change of resistance which occurs when a carbon layer is bombarded. The resistivity is assumed to be given by

$$\rho(x) = \rho_o + A\,\phi\,f\,(x)$$

where ρ_o is the unperturbed resistivity, ϕ is the fluence, A is a proportionality constant, and f(x) is the damage profile induced by the ion or neutral flux. Integrating for total resistance and taking the difference induced by the flux damage one arrives at

$$\Delta R = \frac{A\phi}{d^2} \int_o^d f(x)dx$$

where d is the carbon film thickness. The damage profile f(x), is related to the incident ion energy. The average ion energy may be determined by plotting the resistance as a function of fluence, as shown in fig. 31. We note again that the form of the distribution function must be assumed (Maxwellian or monoenergetic).

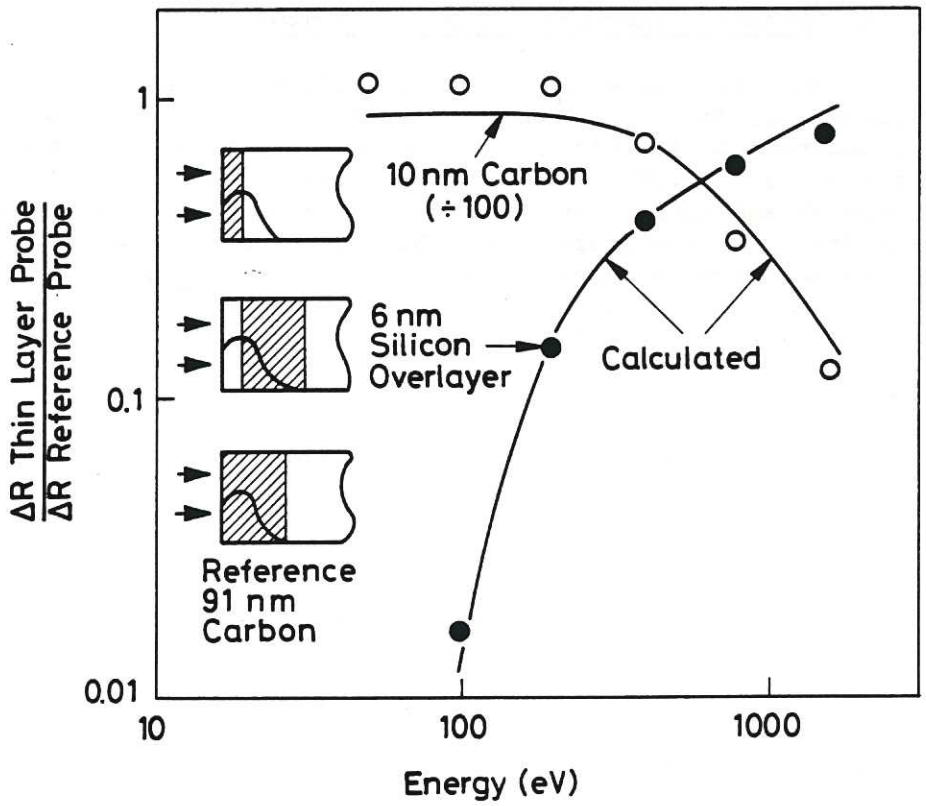

Fig. 32 A comparison of experimental and theoretical estimates of the resistance change in a carbon resistance probe with and without a thin surface layer of silicon.

A variation of this probe is based upon classical foil methods of particle detection[41]. A thin layer of (high resistance) silicon is coated over the carbon as shown in fig. 32. This admits only particles whose energy exceeds a minimum valueselected by varying the Si layer thickness. By comparing the behaviour of two such detectors with different Si thickness (one of which may be conveniently chosen to be zero) it is possible to determine the average particle energy from a single exposure rather than having to carry out multiple exposures until saturation is reached. The behaviour of a 6 nm overlayer is shown in fig. 32. Such a probe has been used on HLT. We note that the distribution function must still be assumed and further variation is required for bimodal or multi-modal distributions. The detector saturates fairly quickly and must be replaced, or possibly regenerated by annealing. The device has very modest power handling capacity (less than a few tens of watts/cm^2) and thus is of little value for sampling the ion flux near the limiter region. In addition the thin overlayers may erode quickly under such a flux. Therefore its use is mostly restricted to applications where a sensitive charge exchange atom detector is required.

5.4 Surface Collectors: Impurity Fluxes

Impurity concentrations are difficult to measure in the plasma boundary. Although emission spectroscopy can be used in principle, it is often difficult to get optical access and interpretation is difficult without a detailed knowledge of the plasma density and temperature profiles. Another possible technique is laser-resonance-fluorescence which has recently been developed into an exremely sensitive and powerful tool which can measure local impurity densities and also, with more difficulty, velocity distributions[87]. The surface collector method is complementary to these techniques in that it allows measurement to be made of the total population of the parallel flux integrated over all charge and excited states. Time resolution can be obtained by a moving collector. The technique is usually applied with the collector surface normal to the magnetic field so that it collects all the flux travelling parallel to the field on the flux tube connected to the collector[88]. The collector surface must itself be free from impurities and again both carbon and silicon have been used. There is a wide variety of methods by which the implanted plasma and impurity species are analyzed. Table 3 taken from McCracken and Stott[89], lists most of the more common techniques. Complete descriptions of these techniques are available in a number of texts[90]. A recent review by Zuhr et al. also discusses these methods[91]. Therefore we will only summarize their use for probe analysis here.

Both SIMS and Auger spectroscopy are suitable for surface analysis. SIMS has very high sensitivity and good depth

Table 3. Surface Analytical Techniques

Technique	Primary beam	Primary energy (keV)	Emergent particle	Elements detected	Minimum detectable concentration (monolayers)	Advantages	Disadvantages
XPS X-ray Photo-electron spectroscopy	X-ray	1-2	Electron	$z \geq 6$	10^{-2}	Sensitive; gives information on chemical structure of surface	Not quantitative
AES Auger Electron Spectroscopy	Electron	2-5	Electron	$z \geq 6$	10^{-3}-10^{-1}	Sensitive; compact; quantitative	Detects only surface layer. Needs calibrating
ISS Ion Scattering Spectroscopy	Ion	1-50	Ion	$z \geq 6$	10^{-3}	Sensitive; gives information on surface structure	Requires primary ion beam. Has to be calibrated. Detects only surface layer
PIXE Proton Induced X-ray	Ion	1 MeV	X-ray	$z \geq 6$	10^{-2}	Sensitive; good element resolution	Has to be calibrated Requires MeV ion beam No depth resolution
RBS Rutherford Back Scattering Spectroscopy	Ion	0.5-10 MeV	Ion	$z \geq 6$	10^{-4}-10^{-3}	High sensitivity; quantitative; depth distribution	Requires MeV ion beam. No light elements. Surface must be reasonably smooth
NRA Nuclear Reaction Analysis	Ion	$\sim$ 1 MeV	Ion X-rays	Selected	Varies with reaction	Depth profile H,D	Limited number of elements. Requires MeV beam
SIMS Secondary-Ion Mass Spectroscopy	Ion	1-5	Ion	Selected	10^{-4}-10^{-2}	High sensitivity; compact Detects H and D	Not quantitative Can be used only for certain elements. Detects only surface layer
SEM Scanning Electron Microscopy	Electron	5.50	Electron	-	-	Surface topography good resolution; $\leq$ 100 A; good depth of focus	-
FR Forward Recoil	Ion	> 300	Ion	Light	10^{-2}	All light elements detected simultaneously	Requires flat surfaces

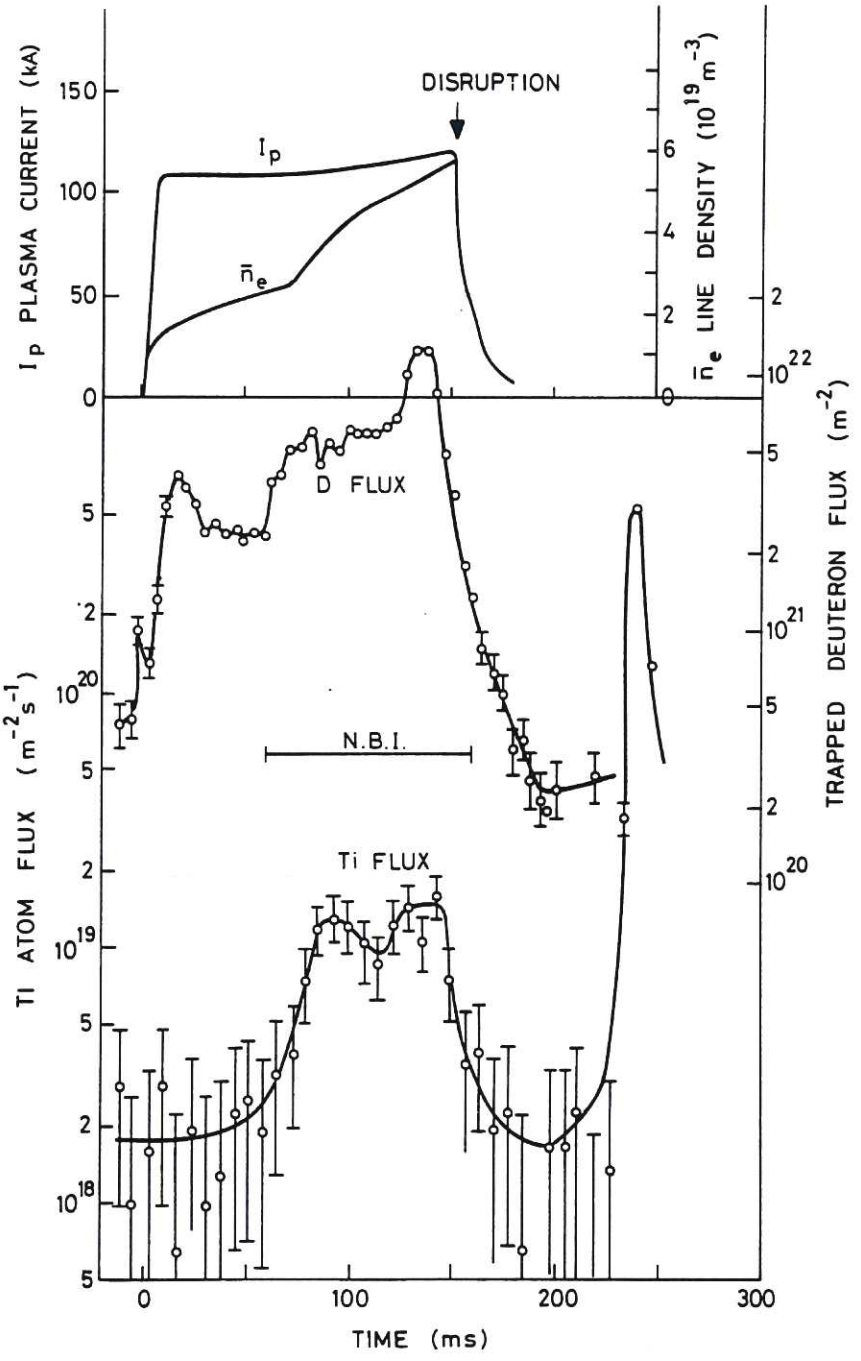

Fig. 33 Measurements of the parallel flux of deuterons and titanium ions as a function of time in the DITE tokamak using a carbon surface collector probe. Both the D^+ and titanium flux increase during <u>hydrogen</u> neutral beam injection.

resolution but it is difficult to make quantitative. Auger spectroscopy, when combined with sputter erosion, has equally good depth resolution and can be quantitative, but it is less sensitive then SIMS. Auger techniques are most useful for the examination of light impurities. For heavy impurities the most frequently used method is Rutherford Backscattering spectroscopy (RBS). RBS is both sensitive and quantitative. It also has the advantage that its sensitivity is proportional to the square of atomic number (Z) so that the high Z impurities which are most deleterious to the plasma are most easily detected. When performed using heavy ion beams (such as ^{14}N) background scattering via light substrates like C can be eliminated[92].

Transfer of samples in atmosphere is possible, although contamination by lead in the atmosphere can be a problem. Air transfer is not satisfactory for low Z impurities such as carbon and oxygen and contamination can occur even with vacuum transfer. Great care has to be taken with the collector and with the vacuum system to overcome this problem. Time resolved measurements of high Z impurities are shown in fig. 33. The impurity flux is normally large during the starting phase[93]. In this case the flux of both impurities and deuterium ions increases during neutral injection[94]. Results for both time resolved fluxes and radial profiles of impurities have been obtained for a number of machines[95-99]. In general the incident metal fluxes at the limiter radius are in the range 10^{18}-10^{19} ions m^{-2} s^{-1}.

The determination of impurity energy and charge state has not yet been satisfactorily solved. The implantation depth profiles are too small for their measurement to be a satisfactory technique. There have been a few attempts to measure the larmor radius by looking at the spatial distribution behind an orifice in a manner similar to that discussed for hydrogen ions c.f. section 5.2[80,83]. This is quite a simple technique in some cases. However, knowing the larmor radius does not give the energy and charge independently. If the impurities are in energy equilibrium with the plasma the energy can be obtained from the plasma ions (necessarily of charge 1) and hence the mean charge state of the impurities can be obtained. Results for titanium impurities in DITE are shown in fig. 34. This technique is rather time-consuming and has not been widely used. However, since the energy and charge state are important parameters in determining impurity sputtering and there are few alternative techniques available, this method must be considered.

In general the surface collector techniques are rather slow. Nevertheless they have the attraction that they allow measurements to be made away from the radiation from the plasma. This may be a very significant factor in their favour during operation with DT reacting plasmas where large fluxes of neutrons

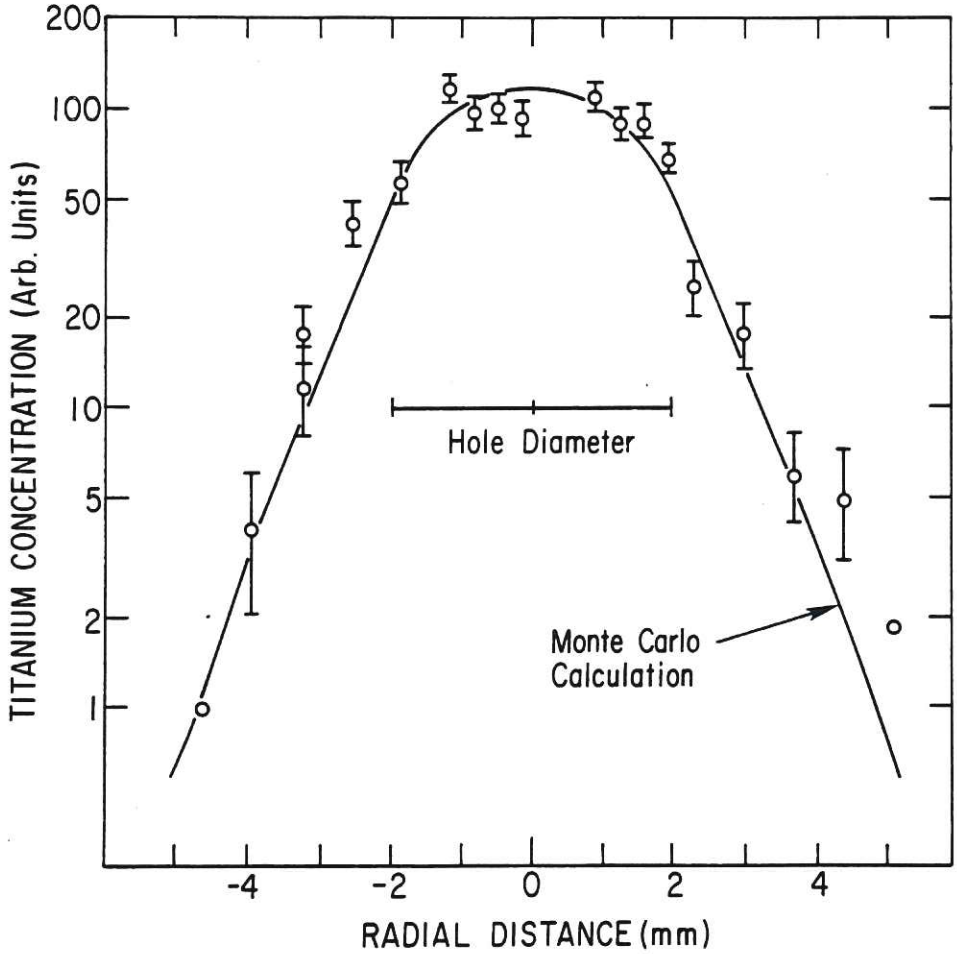

Fig. 34 Experimental measurements of the spatial distribution of titanium atoms on a carbon collector behind a 4 mm diameter hole, compared with a Monte Carlo calculation for 80 eV Ti^{4+} ions.

and gamma rays will occur. The techniques are independent of other plasma parameters and give information about the total flux and the energy with which ions arrive at the surface, which are difficult to obtain in any other way.

5.5 Surface Collector Probes: Alpha Particles

The technique for alpha particle collection is very similar to that for hydrogen isotopes and impurities. Helium ions are tightly bound in the lattices of most materials and their trapping behaviour and range-energy relationship have been studied in great detail[100]. Because they are not present as impurities it is possible to detect very low concentrations. The attraction of the surface collection technique is the possibility of determining

both flux and energy distribution by measuring the depth distribution in the collector.

The depth distribution will give a measure of the alpha particle confinement. The mean depth of a 3.5 MeV α-particle implanted in nickel is 6 μm as compared to the depth of a 20 keV ion which is 0.085 μm[100]. Thus the fraction of the α flux which has not thermalized and contributed to the core heating should be easily distinguished. If the alphas are slowed down in the plasma then it is to be expected that they will ultimately diffuse out with the other plasma ions and hit the limiter. There will only be a very small charge exchange flux to the wall as the cross section for proton charge exchange with helium is typically three

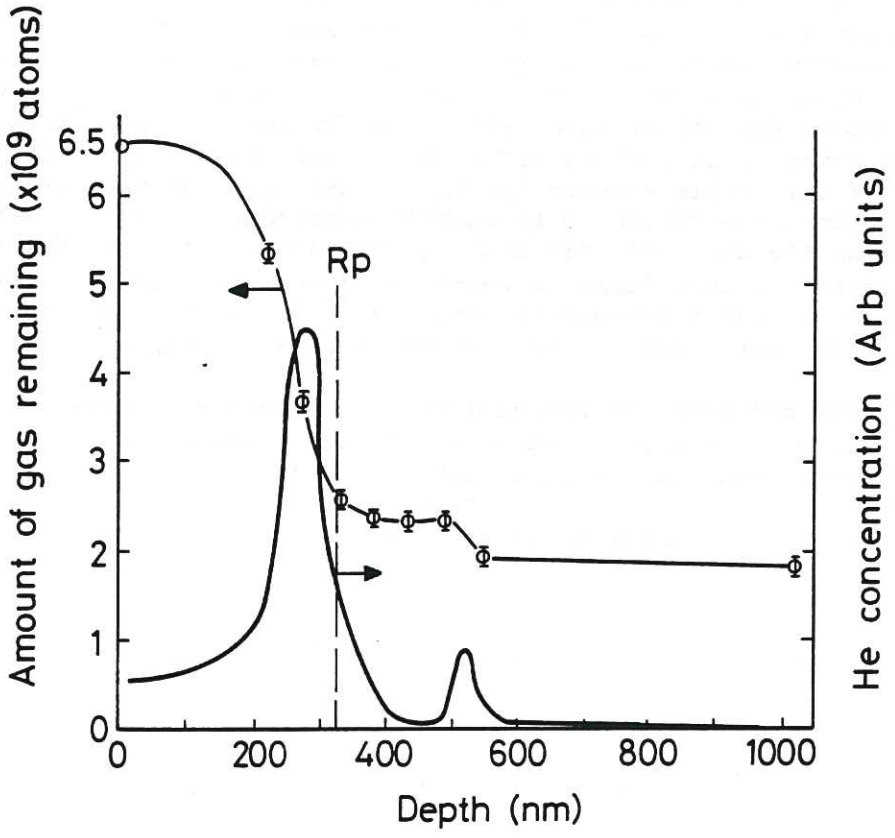

Fig. 35 Depth distribution of helium ions in a nickel foil implanted at 100 keV to a fluence of 2.9×10^{11} atoms cm^{-2}. The measured integral and the derived differential distribution are shown. R_p is the projected range of the He^+ ions in nickel.

orders lower than for hydrogen[101]. The spatial distribution of the α's which are lost before slowing down in the plasma has been discussed by Bauer et al[102]. Their distribution is expected to be very asymmetric, coming out predominantly along the mid plane. Thus collectors placed at intervals around the torus poloidally and toroidally can be used to confirm this asymmetry and to assess both the energy distribution and the spatial distribution of the alpha particles arriving at the wall.

A variety of methods can be used for getting the number and depth distribution of the helium. One of the most sensitive is thermal desorption which in conjunction with surface lapping has been used to determine the depth distribution of 10^{11} atoms cm^{-2} implanted at 100 keV[103]. Results are shown in fig. 35. An alternative is to use nuclear scattering of protons after catching the helium in a thin film[104]. There is a nuclear scattering resonance for helium which significantly enhances the back-scattering cross section above the Rutherford cross section. The use of thin films reduces the backscattering from the substrate and allows the helium to be clearly observed. Using 2.5 MeV protons the depth distributions of 50, 100 and 150 keV ^4He ion implanted in thin films of copper have been analyzed. The sensitivity of this technique is low, $\sim 10^{17}$ atoms cm^{-2}, and is therefore marginally useful for early DT experiments.

The collector technique thus can be used to confirm the overall flux of alphas (which should be consistent with the integrated neutron flux), to determine the degree with which they have been contained by the plasma, and by using a series of collectors around the torus to determine any poloidal or toroidal asymmetries.

6. PROBES FOR EROSION MEASUREMENTS

Erosion of the wall and limiter will take place as a result of a number of different processes including sputtering, arcing and evaporation. Arcing and melting can often be recognized by post exposure analysis but erosion due to sputtering is less easily recognized. It is clear that the erosion rate will vary widely depending on the local plasma and energy fluxes. The removal of wall or limiter material is important not only from the point of view of plasma contamination but also due to the actual change in mechanical strength of tokamak components. Very large erosion rates $\sim$ 10-100 cm yr^{-1} are predicted for the first wall of reactors due to sputtering if light elements e.g. carbon or beryllium, are used. Most eroded material it is hoped will be redeposited[105]. In the steady state in a closed machine on average the net erosion must be near zero. However because of the non-uniformities some redistribution of material is inevitable and

this behaviour has been commonly observed in present tokamaks[106]. Let us consider the simple case where we have an impurity flux Γ_I arriving at a surface at the same time as a plasma flux Γ_p. Neglecting impurity-impurity sputtering and assuming plasma sputtering to be proportional to Y.C where Y is the sputtering yield and C is the impurity surface concentration (assumed < monolayer) then the surface concentration will be given by

$$\frac{dC}{dt} = \Gamma_I - C\,\Gamma_p\,Y$$

$$\text{i.e. } C = \frac{\Gamma_I}{\Gamma_p S}\,[1 - \exp(-\Gamma_p Y t)]$$

Thus the surface concentration will build up linearly and then reach a saturation level given by a balance between incident flux and sputter erosion. Obviously much more complex situations can arise but it is clear that in measuring erosion it is necessary to distinguish as far as possible between erosion and deposition. Making measurements as a function of incident fluence is one way in which this can be accomplished. We now consider some techniques which can be used to make sensitive measurements.

6.1 Thin Film Techniques using Surface Analysis

The thickness of a thin film (~ 20 nm) on a dissimilar substrate can be quite accurately measured using Rutherford backscattering, SIMS or sputter Auger spectroscopy. In successive measurements changes in surface coverage of ~ 10^{19} m^2 can be detected. Using moving probes, time resolution is possible and good spatial resolution using small analysing beams is also straightforward. In addition because RBS detects other elements it is easy to distinguish between erosion of the film and deposition of different atomic species on the surface. Thus if the film is chosen to be an element which is not normally in the tokamak system, it is easy to distinguish between erosion and deposition. This technique has been used with Rutherford backscattering as a sensitive method of measuring sputtering yields[107]. For RBS a heavy film on a light substrate is the simplest to analyse[108]. The major drawback to this technique is that the erosion of the film on a dissimilar substrate may not be representative of bulk material. High heat fluxes may also be perturbing in terms of heating the thin film to high temperatures and possibly causing evaporation.

6.2 Implantation of a Marker Species

This is a development of the thin film approach. Instead of evaporating a thin film a different atomic species is implanted in

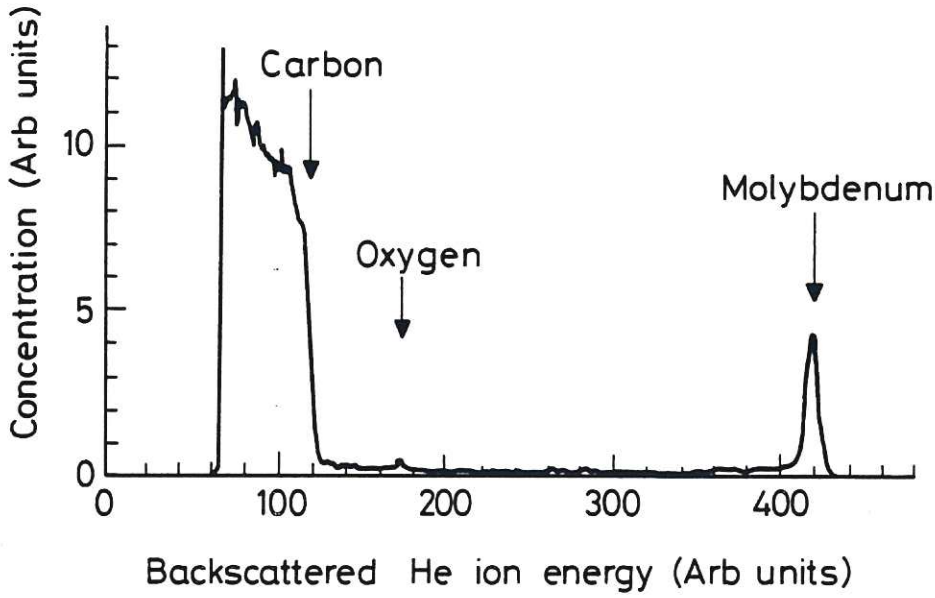

Fig. 36 R.B.S. spectrum of a molybdenum layer on a carbon substrate. A small oxygen impurity peak is also present.

a standard substrate. This marker can be detected by surface analysis and RBS is again a convenient non-destructive technique. A heavy marker in a light substrate such as carbon is easy to see, fig. 36. In this case the position of the marker in the surface is determined from the energy loss of the backscattered atoms in traversing the solid to the marker on the penetrating and backscattered paths. The erosion of the surface is measured by the change in the peak area.

A special case of this technique is the use of an isotopic marker. Implantation of ^{13}C in ^{12}C has been used by Roberto et al[98]. to demonstrate erosion of carbon in the divertor plates of the ASDEX tokamak. The results are shown in fig. 37. The ^{13}C peak was implanted at 35 keV with an incident angle of 45^{o} to a dose of 2×10^{17} ions cm^{-2}. On the control sample the ^{13}C peak is quite clearly separated from the ^{12}C edge. As erosion or deposition occurs the ^{13}C peak moves either away from or towards the ^{12}C edge. A change of about 10 nm in thickness can be detected. The method has again the advantage that any other impurity deposited on the surface can be clearly identified in the RBS spectrum. Measurements of simultaneous erosion and deposition as a function of time are shown in fig. 38. Carbon is clearly eroded during the initial phase of the discharge while iron and titanium are deposited. Later in the discharge there is some indication of carbon deposition.

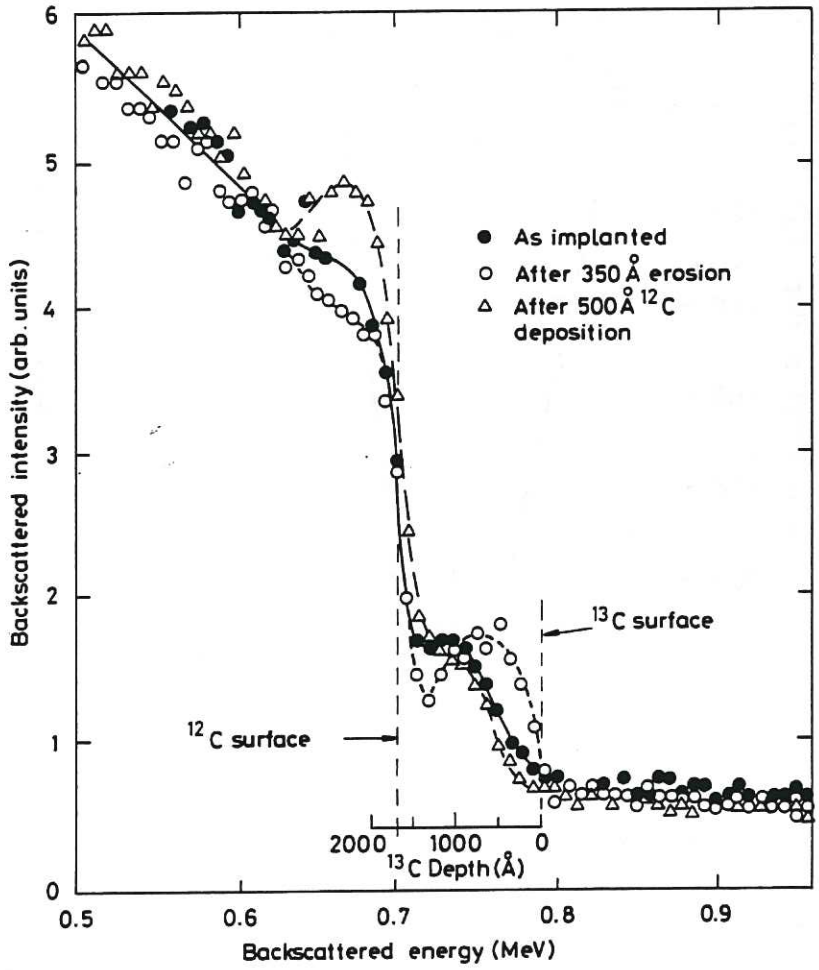

Fig.37 The R.B.S. spectrum of ^{13}C implanted in ^{12}C at 35 keV to a dose of 3 x 10^{17} atoms cm^{-2}, as implanted and after both erosion and deposition of carbon.

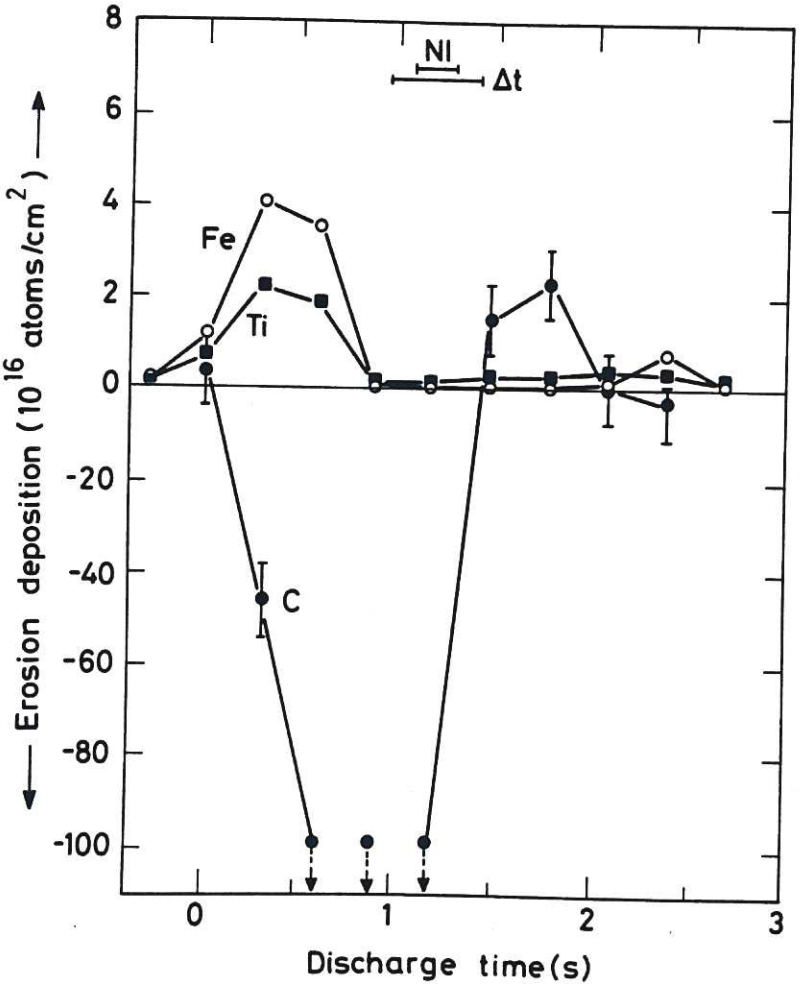

Fig.38 Erosion and deposition as a function of time on a surface collector probe exposed to 10 superimposed discharges in ASDEX with 2.5 MW of neutral beam heating.

6.3 Thin Film Activation

A third method of measuring erosion is to use a nuclear activation technique. By using a nuclear reaction with a sharp energy threshold and using a beam with an energy just above the threshold a thin layer of the surface can be activated. When the incident beam slows down below the threshold energy activation stops. Many (α,n) and (p,n) reactions are suitable, Table 4, and have threshold energies which can be reached with van de Graaff accelerators [109].

Table 4 Isotopic species suitable for thin film activation

	Activation Half Life Days	Activation Energy, MeV
$^{96}Mo(p,n)^{96}Tc$	4.3	7.5
$^{48}Ti(p,n)^{48}V$	16	6.8
$^{56}Fe(p,n)^{56}Co$	78.8	8.2
$^{65}Cu(p,n)^{65}Zn$	244	5.2
$^{12}C(^{3}He,2\alpha)^{7}Be$	53	16.2

These reactions have been used in a wide range of applications[110] including divertor plate erosion[111]. One attraction of the technique is that real time measurements can be made since the activated species are generally γ emitters with energies of 1 to 2 MeV and can be readily detected with a NaI detector outside the vacuum vessel. Another potential advantage is that the redistribution of the eroded material can be easily detected from the activation of collectors some distance away. The technique is in many ways similar to the use of neutron activation but because only a thin surface layer is activated it is both more sensitive and requires much lower total activation levels, typically 10 μ C. The main drawbacks are that being a radioactive technique safety precautions have to be taken and that sensitivity is somewhat less than the RBS techniques. The activated layer has a thickness of 1 - 100 μm and the erosion level which can be measured is $\gtrsim$ 0.1 μm. The technique does not give information directly on whether deposition of other species has occurred. There is no reason however why the two techniques of surface analysis and thin film activation should not be combined.

6.4 Measurement of Eroded Material

Another technique for measuring erosion which has recently been tried[112] is shown in fig. 39. The eroded material is collected and subsequently analysed. In this case electron induced X rays were used. Sputtering from a limiter like probe by ions or from the wall by charge exchange neutrals can be measured. The technique could be used in conjunction with either the thin film activation or the implanted marker techniques.

The above discussion makes it clear that there are many useful experimental approaches to the measurement of erosion. Much wider and more systematic use of these techniques should

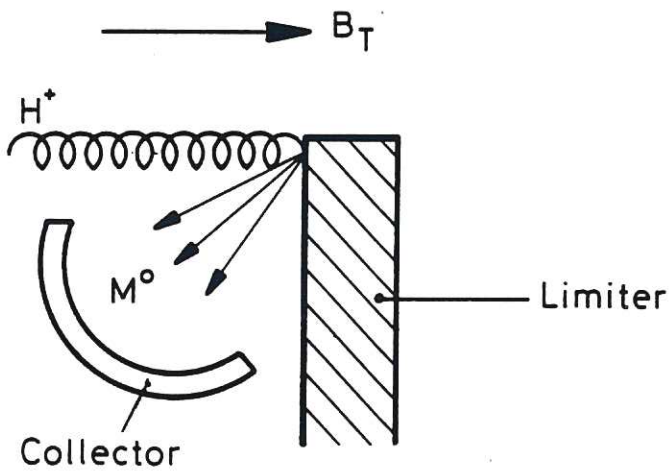

Fig. 39 Schematic of a collector for measuring erosion of the limiter in a tokamak.

result in a better understanding of the processes involved and in better estimates of wall lifetimes. In addition the measurement of erosion rates in conjunction with measurements of incident ion and electron fluxes and energies should give an excellent method of cross checking the validity of various boundary layer models.

7. LONG TERM PROBES

A number of investigations have been made of the condition of tokamak walls after a long period of operation[105]. These show that the material has been widely redistributed by a variety of erosion and redeposition processes. In addition significant physical damage by arcing, melting and evaporation is observed. Careful observations can reveal large non uniformities in the surface interactions. The analyses also indicate that changes in the material properties (particularly surface properties) must have occurred. Such properties including sputtering rates, particle and energy reflection coefficients, secondary electron emission coefficients, etc. are critical inputs to boundary models. Direct measurements of data using samples from the wall would allow an estimate of the error introduced by using the data for pure materials. It is relatively simple to attach samples which can be removed at intervals when access to the torus is possible. Such samples yield a considerable amount of useful data. The sample programme on JET includes:

(1) Examination of samples for physical damage using mainly optical microscope and scanning electron microscope.

Measurement of change of physical properties e.g. surface hardness.

(2) Measurement of impurity deposition and erosion. Methods of measuring erosion have been discussed in section 6.

(3) Measurement of changes in relevant surface properties such as sputtering rate, particle and energy reflection coefficients.

(4) Measurement of the hydrogen and deuterium inventories - to correlate this with the change in surface composition and to try and estimate total incident fluence. This may be obtainable using a diffusion technique proposed by Borgesen et al[114]. The hydrogen or deuterium isotope inventory measurement is particularly important as a cross check for estimates of the tritium inventory during DT operation.

For all these investigations a range of collector materials is desirable - in particular a low Z collector e.g. carbon which can be used to detect the deposition of medium or high Z element deposition; a second clean collector e.g. silicon to measure carbon deposition, and a third probe material which represents the wall material itself. Such probes need only be very simple so that a large number placed in poloidal and toroidal arrays can allow an overall picture of asymmetries. An example of the design for the JET probes is given in fig. 40.

It must be recognized that such probes integrate over a long period of operation and that the resulting surface conditions may possibly depend on the number of malfunctions, e.g. disruptions, or the discharge cleaning technique which is used, rather than on the tokamak discharges themselves. Nevertheless since interpretation of the wall interactions depends in part on knowing the properties of this real wall condition detailed investigations of the type described are highly desirable.

8. CONSTRUCTION OF AND DEPLOYMENT OF PROBES

Section 2 of this chapter discussed the influence of plasma heat flux on probe head materials. If T_e and T_i are known it is possible to calculate a maximum electron density to which any probe material may be exposed c.f. equation 6. In tokamaks, the deployment of probes may be limited by other considerations. Start-up and termination transients frequently involve very high localized heat flux from either runaway or "epithermal" electrons. Disruptions can deliver large amounts of power at otherwise "safe" radii. Thus even using caution in the deployment of probes, experiments frequently end in the incapacitation of the collector element. This requires probes to be very robust.

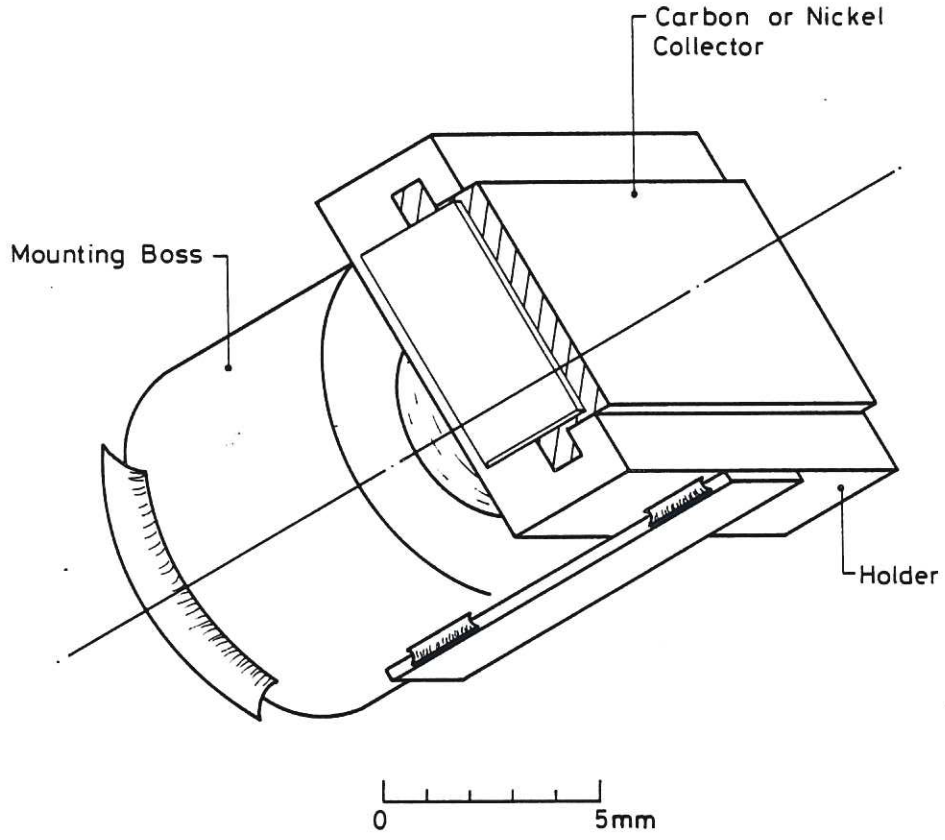

Fig. 40 Schematic of the collector probes used in JET to measure poloidal and toroidal variation of long term deposition erosion and damage.

Fig. 41 shows a comparison of a Langmuir probe once used successfully in the C-stellarator to a triple probe-calorimeter presently in use on TFTR, where terminal disruptions can carry large amounts of stored energy to interior wall components.

The construction of probe transport mechanisms requires the solution of several difficult problems. One must provide a machine vacuum of high quality; current baseline pressures are better than 1×10^{-8} torr and must not be degraded by diagnostic equipment. This usually requires bakeable ($150 < T < 250^{\circ}C$), metal-sealed systems. We note that sample exposure analysis for light impurities places very strict requirements on vacuum. Even at 10^{-8} torr, monolayer coverage by background gas such as CO can occur in as little as ~ 100 seconds.

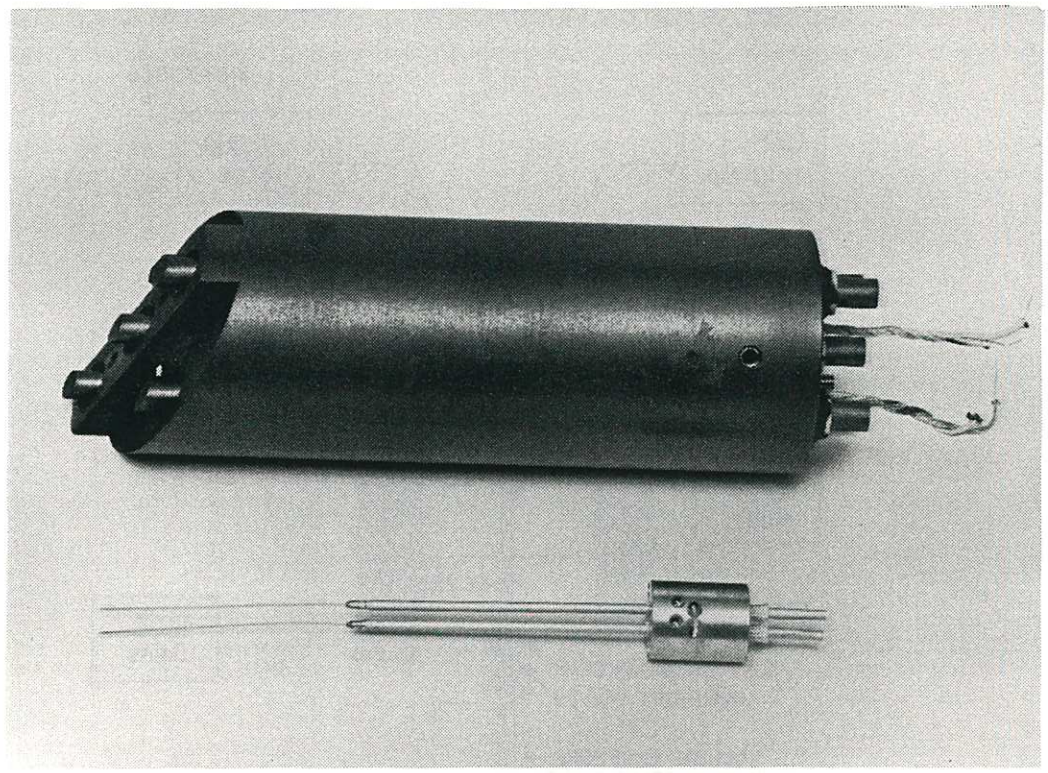

Fig. 41 A comparison of a Langmuir probe used in the C stellerator (1956) with a recent probe from TFTR. The thin collector wires of the former are scarcely visible protruding from their long slender shields.

Probes generally require motion for positioning the head at various locations and often require rotation of the head or motion along a second axis. This requires a means to transmit these motions using drive elements, bearings, and lubricants which are compatible with the UHV requirements.

Electrical signals must be carried from the probe head to the outside. In the case of complicated multi-detector heads (e.g. combined ExB and retarding field analyzer) numerous independent signal paths are required. These must terminate in a small space at the probe head where the material temperature can become very high. Thus special attention to proper insulation material is required to maintain good vacuum. In some cases signals must be transmitted many metres in vacuum and conductors must safely compensate for large motions required by the operation. In future work the environmental requirements are quite difficult to fulfill. Fig. 42 shows present day requirements imposed by D-T operation of TFTR; those for reactor-like operation of JET are even more stringent. One sees that these small signals (on the order of millivolts and milliamps) are being acquired less than a

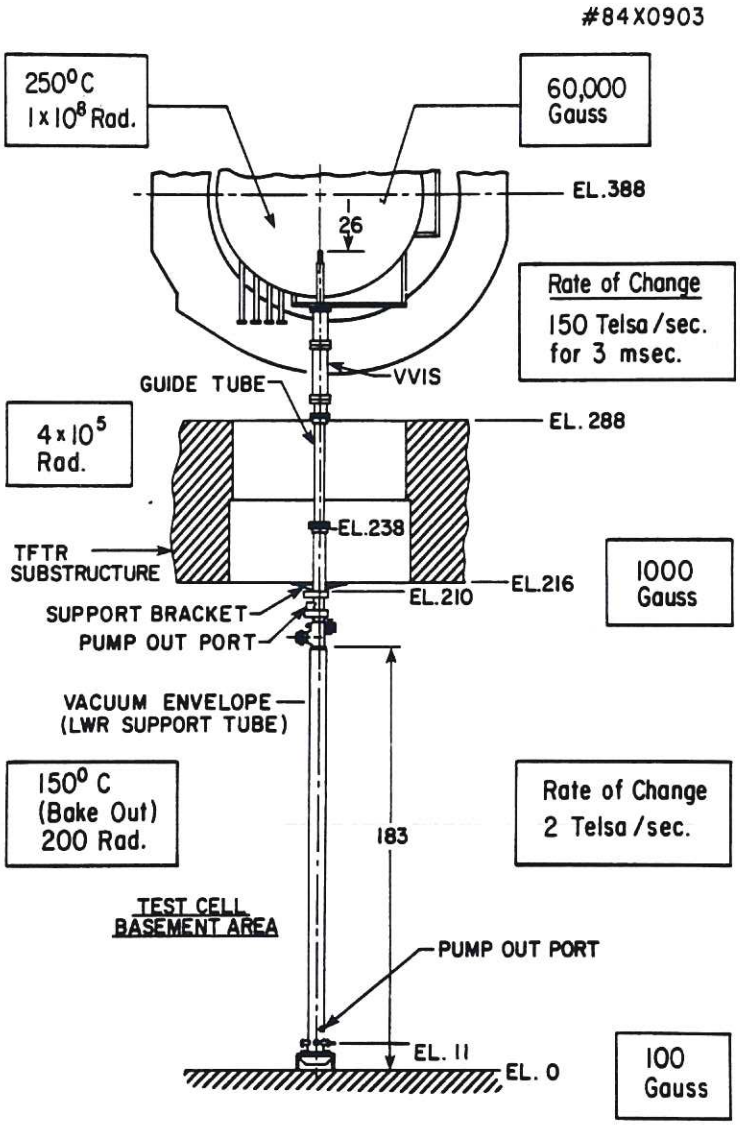

Fig. 42 Schematic diagram showing the requirements for probe operation in TFTR using DT fuel.

metre away from the plasma core where the electro-magnetic interference conditions are severe. Excellent grounding and shielding must be maintained as the probe head moves ~ 5 metres from its rest position.

The solution to these problems cannot be given in general. Each application has its own requirements which are sufficiently

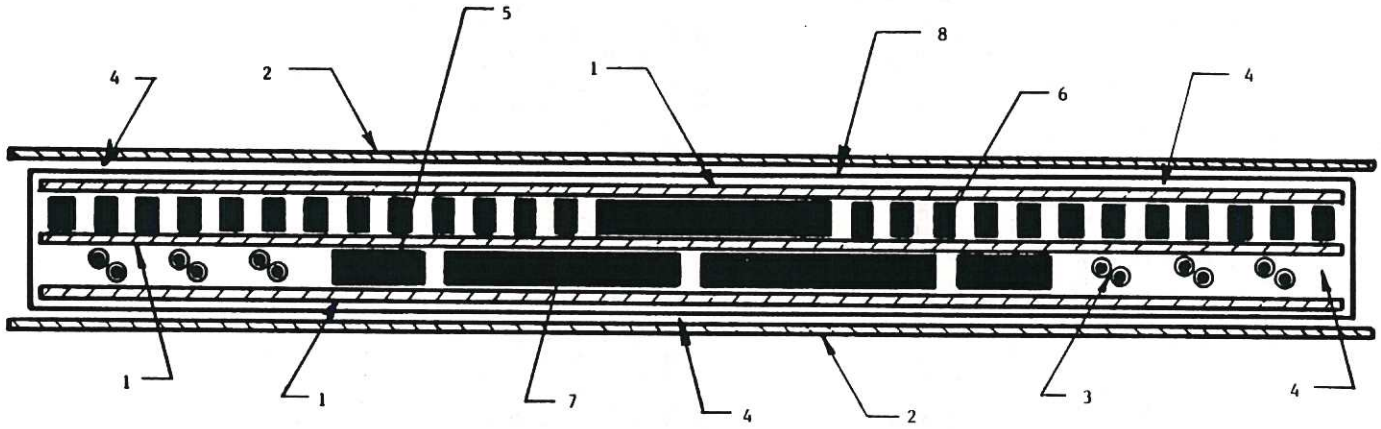

1) 2 MIL KAPTON
2) 1 MIL KAPTON
3) KAPTON COATED MAGNET WIRE IN TWISTED PAIRS, 0.004 IN. DIA. WIRE 0.0003 IN. KAPTON JACKET THICKNESS.
4) .7 MILS ACRYLIC ADHESIVE
5) 5 AMP CONDUCTOR
   1.4 MILS (1 OZ.) COPPER, 0.175 IN. WIDE.
6) .125 AMP TO 1 AMP CONDUCTOR
   1.4 MILS (1 OZ.) COPPER, 0.040 IN. WIDE.
7) 10 AMP CONDUCTOR
   1.4 MILS (1 OZ.) COPPER, 0.450 IN. WIDE.
8) E.M.I. SHIELD
   2300 ANGSTROMS COPPER

Fig. 43 The cross section of the cable used for probes on TFTR.

specific to the confinement device that descriptions of probe drive mechanisms rarely appear in the literature. However, summaries of the solutions for TFTR[115] and JET[113] are available. We treat a few practical problems in the next section.

8.1 High Heat Flux

As shown in fig. 41 one strategy for coping with high heat flux is to make a very large probe nearly entirely from graphite. There are instances where such large probes may be inadmissible, however, and other strategies must be used. One method is to place the probe on a very rapidly moving linear drive. The probe may then be plunged quickly to the desired location and removed quickly. It is also possible to have the probe in place behind a very rugged cover which can be rapidly pulled back a few cm to expose the elements and then replaced. Alternatively, the probe may quickly withdraw a few cm beyond such a stationary shield. One very easy method, already used on PLT, is to rapidly rotate the active elements of the probe (hidden behind apertures) into the flux for a brief period. The same probe allows simple attenuation of the flux by changing the aperture angle between shots.

8.2 Background Noise

There are three major sources of noise or "pick up" in the tokamak environment. The first is rapid fluctuation in the space (or floating) potential of the plasma itself. Such fluctuations are often quite interesting; however in certain measurements they constitute a source of noise. There is little that can be done to reduce this source. The second, magnetic "pick up", can be reduced by careful avoidance of uncompensated loops in the signal path. Tightly twisted pairs of wires in devices such as thermocouples, usually avoids this problem. The third source is tokamak operation electrical systems including auxiliary heating supplies. Avoidance of this source requires attention to proper grounding and shielding techniques. A schematic of the cabling used in the vacuum envelope of the TFTR probes is shown in fig. 43. The wire termination at the probe head requires a continuation of the shielding. Fig. 44 shows a multiconnector coaxial feed-through with which the TFTR probe heads mate. This feed-through is capable of continuous operation up to 400°C.

8.3 Motion

Linear drives in many probe systems involve long distances, for example, the JET fast transfer system, shown in fig. 45, requires a motion of 22 metres. Such motion in this instance will be provided by a railroad-like system of a carriage propelled along an unlubricated track via linear induction motors.

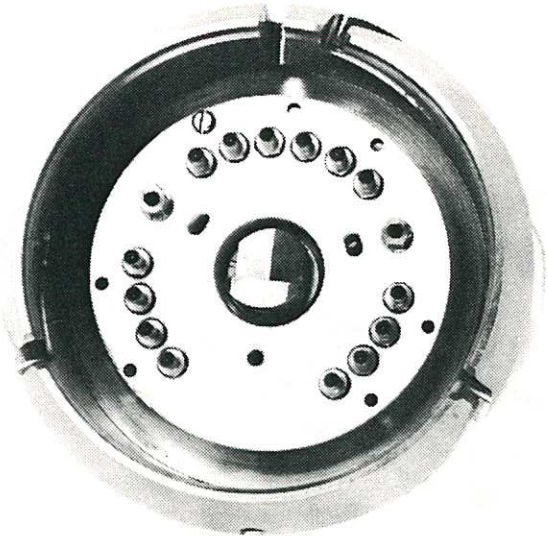

Fig. 44 Multi-connector feed through used for probes on TFTR.

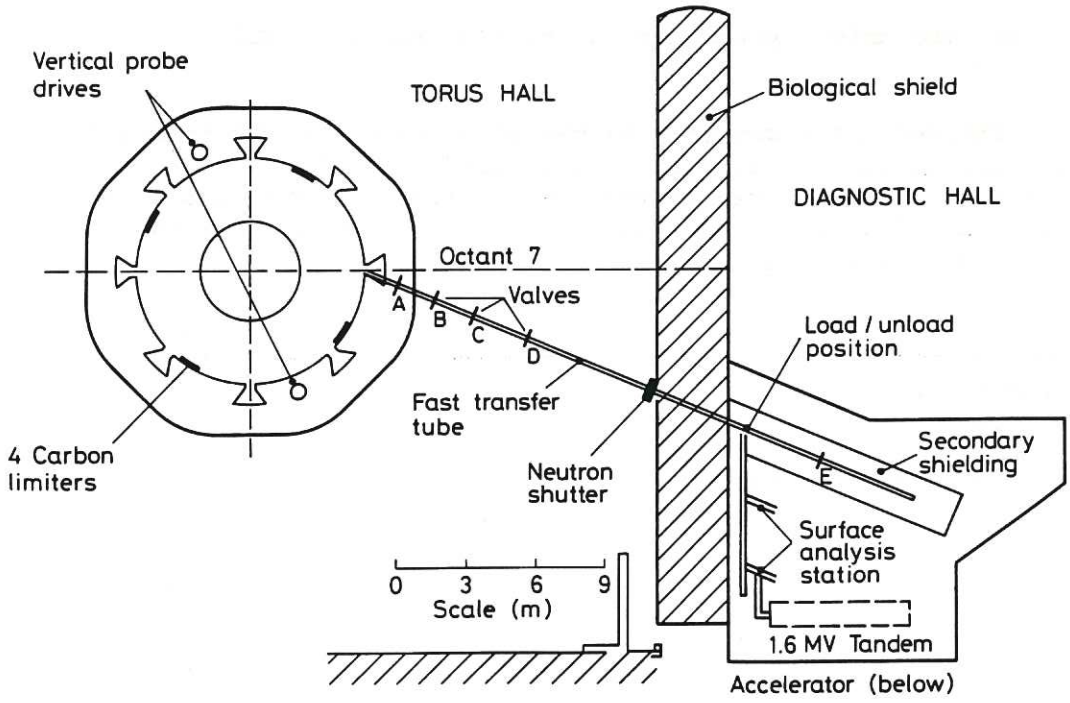

Fig. 45 The layout of the vertical probe drives and the fast transfer system for taking probes from the plasma edge to the surface analysis station on JET.

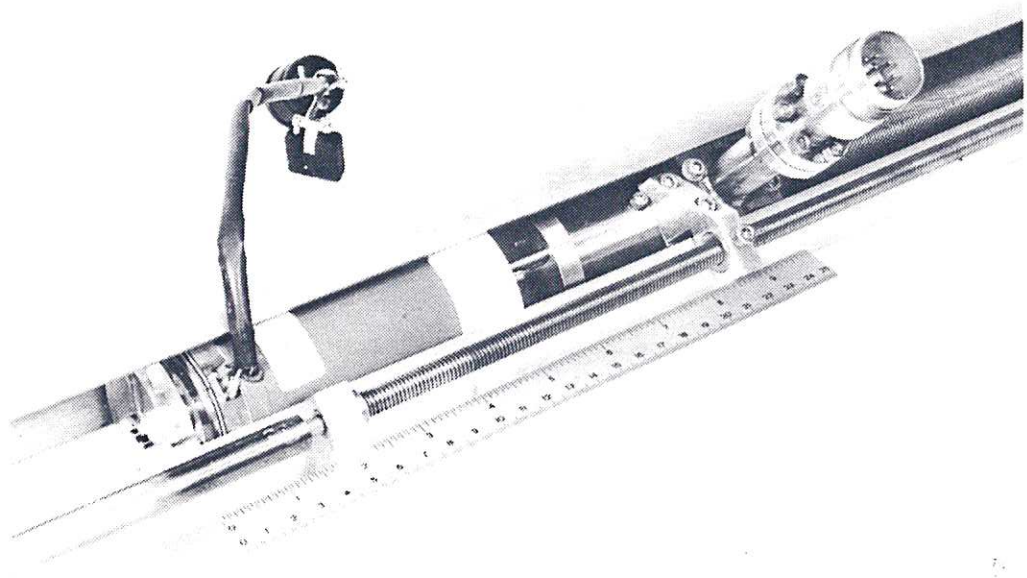

Fig.46 The drive system for moving the probes on PLT.

Shorter distances (5-6 m) may be accommodated by internal rack and pinion drives such as that used on TFTR or external threaded-rod/ball screw drives such as those on PLT and DITE. The latter drives are well-suited to bellows vacuum spaces. A photograph of such a probe is shown in fig. 46.

Lubrication of interior components is a difficult subject. Most commonly, dry lubricants such as MoS_2, WS_2, Ag or Au are employed on bearing balls and races and gear teeth. A combination Ni/MoS_2 dry lubricant has been used successfully for high speed probe bearings on PLT. Excellent results have also been achieved with perfluoropolyethanes such as Bray[116] or Krytox[117]. Whether such lubricants may be safely employed depends on the specific vacuum requirements, operating temperatures and proximity to the plasma. Often it is necessary to reduce loads and speeds and run dry dissimilar materials for bearings and gears.

Rotary motion is normally achieved via bellows sealed (wobble drives, direct drives, etc.) feed throughs. Ferrofluidic feed-throughs have been used for very long life and high loads. These latter require shielding from the magnetic fields of the fusion device. Unfortunately their application is limited as they cannot be baked due to the high vapour pressure of the ferro-fluid.

REFERENCES

1. I. Langmuir and H.M. Mott-Smith, Gen.Elec.Rev. 26, 731 (1923), 27. 449, 583, 616, 726, 810 (1924). Also see I. Langmuir and K.T. Compton, Rev.Mod.Phys. 3, 191 (1931).
2. H. Carslaw and Jaeger, Conduction of Heat in Solids, Oxford Press, Oxford (1959), p 401.
3. H. Vernickel, J.Nucl.Mat. 111 & 112, 531 (1982).
4. L. Schott in Plasma Diagnostics, Ed by W. Lockte-Holtgreven, North Holland, Amsterdam (1968), p 668
5. F.F. Chen in Plasma Diagnostic Techniques, Ed R.H. Huddlestone and S.L. Leonard, Academic Press, New York (1965), p 113.
6. J.D. Swift and M.J.R. Schwar, Electrical probes for plasma diagnostics, Iliffe, London 1970.
7. G.D. Hobbs and J.A. Wesson, Plasma Phys. 9, 85 (1967).
8. P.J. Harbour and M.F.A. Harrison, J.Nucl.Mat. 76 & 77, 513 (1978).
9. P.C. Stangeby, Phys.Fluids 27, 682 (1984).
10. P.J. Harbour, CLM Preprint-535 (1978) unpublished, (available from Culham Lab. on request).
11. P.C. Stangeby, G.M. McCracken, S.K. Erents, J.E. Vince and R. Wilden, J.Vac.Sci. and Technol A1 (1983) 1302.
12. Y. Gomay, N. Fujisawa, M. Maeno, et al., Nuclear Fusion 18 (1978) 849.
13. T. Kobayashi, M. Shimada, S. Sengoku, et al., J.Nucl.Mat. 121 (1984) 17.
14. F. Hoffman, Ch. Hollenstein, B. Joye, et al., J.Nucl.Mat. 121 (1984) 22.
15. D.K. Owens, S.M. Kaye, R.J. Fonck and G.L. Schmidt, J.Nucl.Mat. 121 (1984) 29.
16. R. Budny and D. Manos, J.Nucl.Mat. 121 (1984) 41.
17. G.M. McCracken, S.K. Erents, D.H.J. Goodall, G.F. Matthews, J.W. Partridge, S.J. Fielding and B.A. Powell, J.Nucl.Mat. 128/129 (1984) 150.
18. K. Ertl and the ASDEX team, J.Nucl.Mat. 128/129 (1984) 163.
19. C. Kahn, K.H. Burrell, E. Fairbanks, T. Petrie, M. Shimada, M. Washizu and S. Sengoku, J.Nucl.Mat. 128/129 (1984) 172.
20. B. Lipschultz, et al., to be published.
21. E.O. Johnson and L. Malter, Phys.Rev. 76 (1949) 1411.
22. E.O. Johnson and L. Malter, Phys.Rev. 80 (1950) 58.
23. G. Proudfoot and P.J. Harbour, J.Nucl.Mat. 111 and 112 (1982) 87.
24. M. Kamitsuma, S.L. Chen, J.S. Chang, J.Phys.D. 10, 1065 (1977).
25. S.L. Chen and T. Sekiguchi, J.Appl.Phys. 36 2363 (1965).
26. D.K. Owens and S.M. Kaye, private communication.
27. M.H. Cho, C. Chan, N. Hershkowitz and T. Intrator, Rev.Sci. Instrum. 55, 631 (1984).

28. N. Hershkowitz, B. Nelson, J. Pew and D. Gates, Rev.Sci. Instrum. 53, 29 (1983).
29. S.K. Erents and P.C. Stangeby, J.Nucl.Mat. 111 & 112, 165 (1982).
30. D.M. Manos, R.V. Budny and S.A. Cohen, J.Vac.Sci.Technol., A1, 845 (1983).
31. P.C. Stangeby, Phys. Fluids (1984) in press.
32. P.J. Harbour and G. Proudfoot, J.Nucl.Mat.121 (1984) 222.
33. W. Poschenrieder, private communication.
34. G.M. McCracken and J.H.C. Maple, Brit.J.Appl.Phys. 18 (1967) 919.
35. P. Mioduszewski, L.C. Emerson, J.E. Simpkins, et al., J.Nucl.Mat. 121 (1984) 285.
36. P.C. Stangeby, J.Nucl.Mat. 121, (1984) 36.
37. J.F. Waymouth, Phys.Fluids 7, 1843 (1984)
38. P.C. Stangeby, G.M. McCracken, S.K. Erents and G. Matthews, J.Vac.Sci.Technol. A2 (1984) 702.
39. S.J. Zweben and R.J. Taylor, Nucl.Fusion 21, 193 (1981), 23,513 (1983).
40. P.J. Harbour and G. Proudfoot, IAEA Technical meeting on divertors and impurity control. Editors M. Keilhacker and V. Daybelge, IPP Garching 1981 pg.45.
41. J.E. Osher in Plasma Diagnostic Techniques, eds R.M. Huddlestone and S.L. Leonard, Academic Press, NY (1965).
42. S.S. Medley and D.R.A. Webb, J.Phys.D. 4 (1974) 658.
43. A.W. Molvik UCRL 52981 report Lawrence Livermore Laboratory 1981.
44. P. Staib, J.Nucl.Mat. 93 & 94, 351 (1980).
45. G.F. Matthews, J.Phys.D. 17 (1984) 2243, and private communication.
46. M. Caulton, RCA Review 26, 217 (1965).
47. D.W. Mason, Plasma Physics 6, 553 (1964).
48. S. Stephanakis and W.H. Bennett, Rev.Sci.Instrum. 39, 1714 (1968).
49. J.A. Simpson, Rev.Sci.Instrum.32 (1961) 1283.
50. G. Doucas, Int.J. of Mass Spec and Ion Phys.25(1977)71.
51. D. Manos, R. Budny, T. Satake and S.A. Cohen, J.Nucl.Mat. 111 & 112, 130 (1982).
52. D.N. Arion and R.F. Ellis, Rev.Sci.Instrum. 52 1032 (1982).
53. R.L. Stenzel, R. Williams and R. Aguero, Rev.Sci.Instrum. 53 (1982) 1027.
54. R.G. Chambers, Plasma Physics 14 (1972) 747.
55. Katsumato, Japan, J.Appl.Phys.6 (1967) 123.
56. K. Odajima, H. Kimura, H. Maeda and K. Ohasa, Japan, J.Appl.Phys.17 (1978) 1281.
57. A. de Chambrier, G.A. Collins, P.A. Dupecrex et al., J.Nucl.Mat. 128/129 (1984) 310.
58. F.A. White, Mass spectrometry in Science and Technology, John Wiley, New York, 1969, Chapter 2.

59. A. Gibson, A.S. Bishop, E. Hinnov and F.W. Hoffman, MATT report 261, Plasma Physics Laboratory, Princeton University 1964.
60. H. Kojima, H. Sugai, T. Mori, H. Toyada and T. Okuda, J.Nucl.Mat. 128/129 (1984) 965.
61. S.A. Cohen, J.Nucl.Mat. 76 & 77 (1978) 68.
62. D. Bohm, H. Bishop, H. Massey, in Characteristics of Electrical Discharges, eds Gutherlie and Wakerling, (1949).
63. P.C. Stangeby, J.Phys. B 15, 1007 (1982).
64. G.A. Emmert, R.M. Wieland, T. Mense and J.N. Davidson, Phys.Fluids 23, 803 (1980).
65. S.I. Braginskii, Rev. Plasma Physics 1, 205 (1965).
66. P.E. Staib, J.Nucl.Mat. 111 & 112, 109 (1982).
67. G. Staudenmaier, J. Roth, R. Behrisch, J. Bohdansky, W. Eckstein, P. Staib, S. Matteson and S.K. Erents, J.Nucl.Mat.84(1979)149.
68. S.A. Cohen and G.M. McCracken, J.Nucl.Mat. 84, 157 (1979).
69. W.R. Wampler, D. Brice and C. Magee, J.Nucl.Mat. 102, 304 (1981).
70. W.R. Wampler and C. Magee, J.Nucl.Mat. 103 & 104, 509 (1981).
71. S.A. Cohen, H.F. Dylla, W.R. Wampler and C.W. Magee, J.Nucl.Mat. 93 and 94 (1980) 109.
72. C. Sofield, G.M. McCracken, L.B. Bridwell et al., Nucl.Instrum and Meth. 191 (1981) 383.
73. J. Roth, P. Varga, A.P. Martinelli et al., J.Nucl.Mat. 111 and 112 (1982) 123.
74. K.B. Axon, J. Burt, S.K. Erents, et al. The Bundle divertor: A review of experimental results Culham Laboratory Report CLM R235 (1983).
75. J.S. Ziegler et al., Nucl.Instr.Methods 149, 19 (1978).
76. K. Erents, G. McCracken, J. Vince, J.Nucl.Mat. 76 & 77, 623 (1978).
77. G.G. Ross, et al., J.Nucl. Mat. 128/129 (1984) 730.
78. W.R. Wampler, S.T. Picaux, S.A. Cohen, H.F. Dylla, G.M. McCracken and S.Rossnagel, J.Nucl.Mat. 85 & 86, 983 (1979).
79. W.R. Wampler, S. Cohen, D. Manos, C. Magee, J.Vac.Sci. Technol. 20, 1234 (1982).
80. G. Staudenmaier, P. Staib, W. Poschenreider, J.Nucl.Mat. 93 & 94, 121 (1980).
81. R.Krawec, NASA Technical Note - NASA-TN-D5746, April 1970.
82. R. Zuhr, R.E. Clausing, L. Heatherly and R.K. Richards, J.Nucl.Mat. 111 & 112, 177 (1982).
83. C.J. Sofield, G.M. McCracken et al., Nucl.Inst.Methods 191, 1983 (1981).
84. W. Wampler, Appl.Phys.Lett. 41, 335 (1982).
85. W. Wampler and D. Manos, J.Vac.Sci.Technol. A1, 827 (1983).
86. P.L.F. Hemment, in Ion Implantation Techniques, eds.H. Ryssel and H. Glawischnig, Springer-Verlag, NY (1982) p 209.
87. E. Hintz, J.Nucl.Mat. 93 & 94, 86 (1980). See also present volume chapter by Hintz.

88. P. Staib, R. Behrisch, W. Heiland and G. Staudenmaier, Proc.7th Europ.Conf. on Controlled Fusion and Plasma Physics, Lausanne (1975)p.133.
89. G.M. McCracken and P.E. Stott Nuclear Fusion 19(1979) 889.
90. J.C. Riviere, Phil. Trans. Roy. Soc. A305 (1982) 545; D. Briggs and M.P. Seah Editors, "Practical Surface Analysis" John Wiley 1983.
91. R.A. Zuhr, J.B. Roberto and B.R. Appleton, Nuclear Science Applications 1 (1984) 617.
92. G. Dearnaley, G.M. McCracken, J.F. Turner and J. Vince, Nuclear Instrum & Meth. 149(1978) 253.
93. G.M. McCracken, G. Dearnaley, R.D. Gill et al., J. Nucl, Mat 76 & 77 (1978) 431.
94. G.M. McCracken, J.W. Partridge, S.K. Erents et al., J. Nucl.Mat. 111 and 112 (1982) 159.
95. Y. Hori, A. Sagara, Z. Kabeya, J.Nucl.Mat. 111 and 112 (1982) 137.
96. W.R. Wampler, S.T. Picraux, S.A. Cohen et al., J.Nucl.Mat. 93 and 94(1980) 139.
97. H. Wolff, H. Grote, D. Hildebrandt and M. Laux, J.Nucl.Mat. 128/129 (1984) 219.
98. J.B. Roberto, J. Roth, E. Taglauer and O. Holland, J.Nucl.Mat. 128/129 (1984) 244.
99. E. Taglauer, J.Nucl.Mat. 128/129 (1984) 244.
100. J.F. Ziegler,ed., Helium: Stopping Powers and Ranges in all Elemental Matter , Pergamon Press, NY (1978).
101. R.L. Freeman and E.M. Jones, Culham Laboratory report R 137 (1974) Atomic Collision Processes in plasma physics experiments.
102. W. Bauer, K.L. Wilson, C.L.. Bisson, L.G. Haggmark and R.J. Goldston, Nuclear Fusion 19 (1979) 93.
103. S.E. Donnelly, D.S. Whitmell, R.F. Nelson, AERE-Harwell, Report R 7955 (1975).
104. R.S. Blewer, Appl. Phys. Lett. 23, 593 (1973).
105. Ref. 89 page 938.
106. G. Staudenmaier, P. Staib and G. Venus, J. Nucl. Mat. 76 and 77 (1978)
107. R. Weissman and R. Behrisch, Rad.Effects 19 (1973) 69.
108. G. Mezey, J.W. Partridge and G.M. McCracken, Fusion Technology 6 (1984) 459.
109. P.M. Read, J. Asher, T.W. Conlon and C.J. Sofield, J.Nucl.Mat.99 (1981) 235.
110. T.W. Conlon, Wear 29 (1974) 69.
111. D.H.J. Goodall, T.W. Conlon, C. Sofield and G.M. McCracken, J. Nucl. Mat. 76/77 (1978) 492.
112. G. Staudenmaier, J.Vac.Sci.Tech. (1985) to be published.
113. D.H.J. Goodall, W.O. Hoper, G.M. McCracken, R. Behrisch et al., J.Nucl.Mat. 93/94 (1980) 383.
114. P. Borgesen, B.M.V. Scherzer and W. Möller, J.Nucl.Instrum. and Meth. B (1984) in press.

115. R. Mastronardi, R. Cabral and D. Manos, Proc. NASA 16th Aerospace Mechanism Conf. Pub. 2221 (1982) p 265.
116. Bray Oil Co., Los Angeles, CA 90032.
117. E.I. Dupont, Wilmington, Delaware.